A Szilikátipari Tudományos Egyesület lapja

építőanyag

Journal of Silicate Based and Composite Materials

A TARTALOMBÓL:

2025/2

Central European Congress on Concrete Engineering

vodiCCCe 2026

15th Central European Congress on Concrete Engineering
Vodice, Croatia
5-7/10/2026

We are pleased to announce the upcoming 15th Central European Congress on Concrete Engineering, to be held in the beautiful coastal town of Vodice in Croatia. This year's theme "Sustainable and Innovative Engineering Solutions for Concrete Design Challenges and Practices" will bring together experts, researchers, academics, and industry professionals to explore advanced approaches, share experiences, and inspire future developments. Whether you are involved in design, construction, research, or policy-making, this congress is an excellent opportunity to connect, collaborate, and contribute to the advancement of concrete engineering across Central Europe and beyond.

We look forward to welcoming you to Vodice for an engaging and inspiring event!

CONGRESS TOPICS

1. Materials
2. Concrete structures, including precast and composite structures
3. Design and analysis of concrete structures
4. Technology and construction methods
5. Sustainability, life cycle assessment and climate change adaptation
6. Maintenance, protection, rehabilitation and strengthening
7. Hazards (explosion, floods, earthquake, fire, storms, landslides, winds)
8. Advances in concrete structures (automation, digital fabrication, robotics, additive manufacturing, design process optimization, AI and BIM)

https://sites.google.com/arhitekt.hr/ccc-2026-vodice/home

aci fib CEB-FIP rilem

ACI-*fib*-RILEM Workshop Call

September 28 to 30, 2026
Budapest, Hungary

ACI-*fib*-RILEM 2026 FRC WORKSHOP BUDAPEST

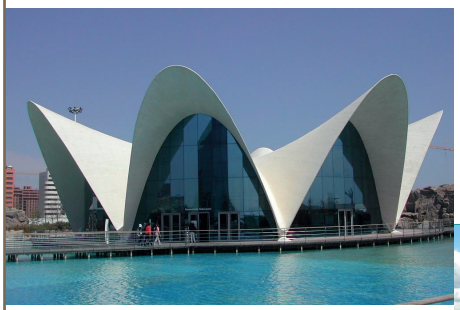

Steel fiber reinforced concrete thin shell structure
Oceanographic Park Restaurant. *City of Arts and Sciences*, Valencia (2002)
Based on blueprint of Felix Candela, by: A. Domingo, C. Lázaro, P. Serna

fib CEB-FIP Hungary

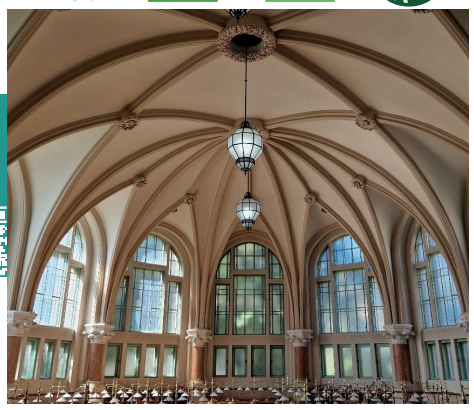

Library of the Budapest University of Tecnology and Ecconomics

Venue – BME Budapest

Budapest University of Technology and Economics was founded in 1782 and it has been regarded as Hungary's number one technical higher education institution for more than 240 years.

Budapest, resting gracefully along the Danube, harmonizes centuries of history with a vibrant present. Landmarks like Buda Castle and Matthias Church echo tales of the past, while District VII's lively atmosphere embodies modern creativity in its eclectic bars and cafes. Art and culture thrive here, from the grandeur of the Hungarian State Opera House to the avant-garde exhibitions at the Ludwig Museum.

Topics

1. Design specifications for applications
   - A. *fib* Model Code 2020
   - B. Standards and design specifications
   - C. Enhanced material behaviour and modelling
   - D. Enhanced structural behaviour and modelling in reinforced and in prestressed concrete members
2. Structural applications
   - A. Buildings, Bridges, Foundations
   - B. Tunnels
   - C. Prefabrication
   - D. Concrete industrial floors
3. Sustainability, Durability, Serviceability
   - A. Design aspects for sustainability and durability. Life Cycle Assessment.
   - B. Serviceability aspects: cracking, ~~first crack,~~ crack pattern, spacing of cracks, crack widths, increase of crack width
4. Design aspects for long term and extreme loads
   - A. Long term behaviour and modelling for shrinkage, creep, fatigue
   - B. FRC under fire, impact or blast loading.
5. Retrofitting and strengthening of existing structures
6. Fibres in new types of concretes and in 3D printed concretes

Sponsorship opportunities

We offer levels of sponsorship: Diamond (8,000 EUR), Gold (5,000 EUR), Silver (2,500 EUR), and Standard (1,000 EUR). Diamond and Gold sponsors receive exhibition space (larger for diamond). Diamond, Gold and Silver receive complimentary workshop registrations (4 for Diamond, 3 for Gold and 2 for Silver). All sponsors will have their logo displayed and name acknowledged during the opening and closing ceremonies, in the workshop proceedings, and on-site materials such as flyers and roll-ups. To become a sponsor, please provide your company details, and the sponsorship fee must be transferred prior to the workshop.
Additionally a Platinum sponsorship level is also considerded and prize is assigned on special topic proposed by the Sponsor.

Contact information

Official website:
https://frcworkshop2026.bme.hu
Műegyetem 3, Budapest, H-1111 Hungary
frcworkshop2026@emk.bme.hu

építőanyag
Journal of Silicate Based and Composite Materials
2025/2

TARTALOM

CONTENT

A finomkerámia-, üveg-, cement-, mész-, beton-, tégla- és cserép-, kő- és kavics-, tűzállóanyag-, szigetelőanyag-iparágak szakmai lapja
Scientific journal of ceramics, glass, cement, concrete, clay products, stone and gravel, insulating and fireproof materials and composites

A folyóiratot referálja · The journal is referred by:
ProQuest · Google Scholar · INDEX COPERNICUS INTERNATIONAL · THOMSON REUTERS

A folyóiratban lektorált cikkek jelennek meg.
All published papers are peer-reviewed.
Kiadó · Publisher: Szilikátipari Tudományos Egyesület (SZTE)
Elnök · President: ASZTALOS István
1034 Budapest, Bécsi út 120.
Tel.: +36-1/201-9360 ▪ E-mail: epitoanyag@szte.org.hu
Tördelő szerkesztő · Layout editor: NÉMETH Hajnalka
Címlapfotó · Cover photo: BIRÓ András

WWW.EPITOANYAG.ORG.HU
EN.EPITOANYAG.ORG.HU

Online ISSN: 2064-4477
Print ISSN: 0013-970x
INDEX: 2 52 50 ▪ 77 (2025) 29-60

Vol. 77, No. 2

Review article: Prospects for creating building materials based on regolith

R. V. KRYVOBOK ▪ Kharkiv Polytechnic Institute, National Technical University, Ukraine ▪ krivobok491@gmail.com
G. V. LISACHUK ▪ Kharkiv Polytechnic Institute, National Technical University, Ukraine ▪ georgiy.lisachuk@khpi.edu.ua
O. Y. FEDORENKO ▪ Kharkiv Polytechnic Institute, National Technical University, Ukraine ▪ olena.fedorenko@khpi.edu.ua
O. R. TYMCHENKO ▪ Kharkiv Polytechnic Institute, National Technical University, Ukraine ▪ sasha.timchenko.94@gmail.com
O. S. RIABININ ▪ Kharkiv Polytechnic Institute, National Technical University, Ukraine ▪ oleksandr.riabinin@ihti.khpi.edu.ua
V. V. VOLOSHCHUK ▪ Kharkiv Polytechnic Institute, National Technical University, Ukraine ▪ valenty93vol@gmail.com
K. Yu. PERMIAKOV ▪ Kharkiv Polytechnic Institute, National Technical University, Ukraine ▪ kostiantyn.permiakov@ihti.khpi.edu.ua
D. A. KUDII ▪ Kharkiv Polytechnic Institute, National Technical University, Ukraine ▪ dmytro.kudii@khpi.edu.ua
I. I. HUMENNYI ▪ Kharkiv Polytechnic Institute, National Technical University, Ukraine ▪ ihor.humennyi@ihti.khpi.edu.ua

Érkezett: 2025. 04. 10. ▪ Received: 10. 04. 2025. ▪ https://doi.org/10.14382/epitoanyag-jsbcm.2025.5

Abtsract

The article discusses the prospects for using lunar regolith for space construction with a promising approach to ensuring a sustainable human presence on the Moon and beyond. The key concept involves the use of resources in place, where local materials such as regolith are used to reduce the need to transport materials from Earth. As a building material, regolith can be processed to create durable building materials using 3D printing and other methods such as melting or sintering. Regolith structures can protect astronauts from extreme temperatures, radiation, and micrometeorites. Regolith contains oxygen, which can be extracted for life support and fuel production. It also contains metals, such as iron, aluminum, and titanium, which can be used to create tools and infrastructure. Construction based on regolith will contribute to the creation of self-sufficient infrastructure on the Moon and Mars. The ability to use local resources to create living quarters, produce oxygen, and generate energy will minimize dependence on supplies from Earth. Current research focused on improving the methods of mining and processing regolith, as well as on the development of new composite materials for space construction, is analyzed. These innovations may also be applicable to Mars and other celestial bodies. The prospects for the development of regolith-based materials for extraterrestrial construction are extremely important for future space missions and the colonization of other planets. The use of regolith makes it possible to build infrastructure, provide energy and life support needs, making human settlements on the Moon and Mars a reality. The development of technologies for the use of this material will continue, creating new opportunities for space exploration.

Keywords: space engineering, silicate, chemical properties, modelling extraterrestrial construction
Kulcsszavak: űrmérnökség, szilikát, kémiai tulajdonságok, földön kívüli építkezés modellezése

Ruslan KRYVOBOK
Ph.D, Doctor of Sciences. Specialist in material sciences of new special-purpose ceramic materials and coatings. Deputy Head of Scientific and Research Part NTU "KhPI".

George LISACHUK
Doctor of Sciences, full Professor. Specialist in material sciences of resource saving and energysaving technologies, new structural ceramic materials and coatings. Head of Research department of NTU "KhPI".

Olena FEDORENKO
Doctor of Sciences, full Professor NTU "KhPI". Fields of interests: chemical technology of functional ceramics and protective coatings.

Oleksandr TYMCHENKO
Ph.D. student, NTU "KhPI", Department of technology of ceramics, refractories, glass and enamels. Specializes in the study of radiotransparent ceramic materials.

Oleksandr RIABININ
Ph.D. student, NTU "KhPI", Department of technology of ceramics, refractories, glass and enamels. Specializes in the study of radiotransparent ceramic materials.

Valentyna VOLOSHCHUK
Research Scientist of the Research Department of NTU "KhPI", Department of technology of ceramics, refractories, glass and enamels. Specializes in the study of radiotransparent ceramic materials.

Kostiantyn PERMIAKOV
Ph.D. student, NTU "KhPI", Department of technology of ceramics, refractories, glass and enamels. Specializes in the study of radiotransparent ceramic materials.

Dmytro KUDII
Ph.D. student, NTU "KhPI", Department of technology of ceramics, refractories, glass and enamels. Specializes in the study of radiotransparent ceramic materials.

Ihor HUMENNYI
Ph.D. student, NTU "KhPI", Department of technology of ceramics, refractories, glass and enamels. Specializes in the study of radiotransparent ceramic materials.

1. Introduction

Today, the study of extraterrestrial bodies is one of the main activities of the largest national space agencies and commercial aerospace companies. Over the past 100 years, humanity has reached the Moon and Mars. The Moon is currently the most explored extraterrestrial object. For a long time, the exploration of the Earth's satellite was limited by the high cost of missions and the lack of resources for a long stay of humans on the Moon.

The prospect of a multi-planetary future for humanity has become more attainable thanks to significant investments and innovations in the aerospace industry. The European Space Agency (ESA) and the National Aeronautics and Space Administration (NASA) have announced their commitment to provide opportunities for people to live permanently in special habitats on the Moon or Mars by 2040. NASA's Artemis program aims to land astronauts on the Moon to create a permanent human presence and support scientific research. In addition, these missions will serve as a testbed for technologies that will be used for future missions to Mars. Long-term human presence on the Moon to accelerate research requires the creation of a developed infrastructure using available resources, including lunar rocks.

The study of lunar rocks has shown that the most accessible local material is lunar soil, the composition of which varies slightly depending on the sampling site (*Fig. 1*). Lunar soil

(regolith) is a layer of loose, heterogeneous material that covers the lunar surface and can reach a thickness of up to 15 meters. It consists of dust, rock fragments, micrometeorites, and the remains of other space bodies that have been bombarding the Moon for billions of years. Unlike the Earth, the Moon has no atmosphere, so all meteorite impacts do not dissipate but leave traces in the form of regolith [1].

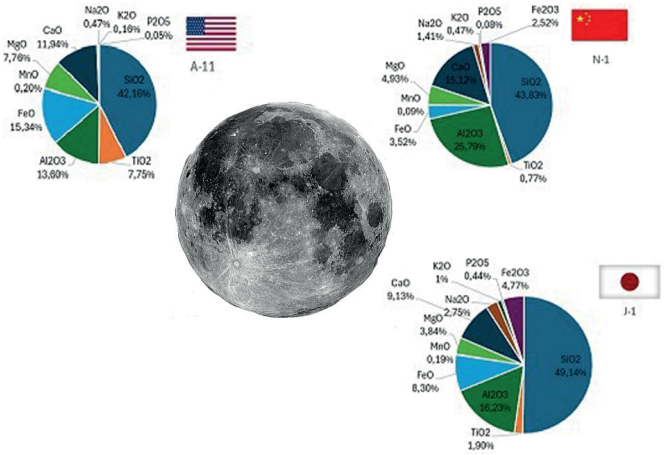

Fig. 1 Illustration of the results of lunar soil studies by various space missions based on simulations according to [3,4,5]
1. ábra A Holdtalaj különböző űrmissziók általi vizsgálatainak eredményeinek illusztrációja [3,4,5] szerinti szimulációk alapján

Modern terrestrial technologies allow for the creation of strong and durable building materials, but due to the high cost of transportation to the Moon, their production must be carried out directly on site from lunar rocks. According to the vast majority of researchers, regolith has great potential for use as a building material due to its availability and useful properties: resistance to high temperatures and extreme temperature changes, chemical inertness, and the ability to protect against radiation [2].

The use of extraterrestrial resources, such as lunar regolith, to build infrastructure on the Moon is a key aspect to ensure the sustainable and affordable development of lunar bases. This will reduce the cost of missions, reduce dependence on transportation of materials from Earth, and make it possible for people to live on the Moon for a long time.

2. Analysis of research and publications

2.1 Chemical and mineral composition of lunar regolith

Real lunar regolith is complex in composition and usually contains large amounts of basalt fragments and their minerals such as pyroxene, olivine, and ilmenite, while those collected from the highlands contain numerous fragments of anorthosite rocks and plagioclase feldspar [6]. In addition, micrometeorite impacts create tiny glass beads that are often found in regolith.

It should be noted that mineral building materials produced on Earth require a large amount of water and significant energy consumption, which makes it impossible to use them on extraterrestrial objects [7]. Unlike terrestrial soil, lunar regolith does not contain organic materials or water. It is completely dry and lacks the biological activity that characterizes terrestrial soil.

It is quite clear that to prepare samples of building materials made from regolith, access to the appropriate amount of raw materials is very limited. Therefore, an important element of research is the creation of mixtures that imitate the mineral composition of lunar regolith. Preparation of simulants is a difficult task, firstly, because of the need to take into account a large number of characteristics, not only possible changes in the chemical composition of rocks sampled in different areas of the Moon, and secondly, because of the limited availability of relevant data.

The most important characteristics of any rock (apart from morphological features) are its chemical and mineralogical compositions, mechanical and physical properties.

The chemical composition of the lunar regolith samples and simulants according to [3-5, 8-10] is given in *Table 1*.

Sample code	Component content per calcined substance, wt. %										
	SiO_2	TiO_2	Al_2O_3	FeO	MnO	MgO	CaO	Na_2O	K_2O	P_2O_5	Fe_2O_3
A-11	42.16	7.75	13.60	15.34	0.20	7.76	11.94	0.47	0.16	0.05	–
A-16	45.20	0.58	26.40	5.29	0.70	6.10	15.32	0.52	0.14	0.12	–
NU-LHT	46.60	0.12	21.55	5.08	0.09	9.50	12.60	0.97	0.12	0.07	–
C-1	49.24	1.910	15.80	11.47	0.14	8.72	7.25	3.08	1.03	0.30	–
J-1	49.14	1.9	16.23	8.3	0.19	3.84	9.13	2.75	1.00	0.44	4.77
N-1	43.83	0.77	25.79	3.52	0.09	4.93	15.12	1.41	0.47	0.08	2.52

Table 1. Chemical composition of lunar regolith samples and simulants according to the results of works. [3-5,8-10]
1. táblázat A holdi regolit minták és szimulánsok kémiai összetétele az irodalmi eredmények alapján. [3–5,8–10]

A similar feature can be found in the samples, namely, a large proportion of SiO_2, which indicates the potential of extraterrestrial regolith for the preparation of building materials. Silicon dioxide is the main component, which indicates the presence of silicates, the most common minerals in lunar regolith. The high content of titanium dioxide in some samples (A-11) indicates basaltic rocks from lunar seas that are rich in ilmenite. Aluminum oxide is often associated with plagioclases, such as anorthosite, which are characteristic of the lunar crust. A high content of iron oxide indicates the presence of iron-bearing minerals such as ilmenite, pyroxenes, and olivine. Low alkaline oxide content is typical for lunar rocks, as they are poor in volatile elements.

We should note that all samples of regoliths simultaneously contain oxides of CaO, FeO, Al_2O_3, and SiO_2 in large quantities (over 10 %). In addition, certain samples (A-11, NU-LHT) also contain a significant amount of MgO and TiO_2 oxides. The authors of [14] proposed the concept of creating new multicomponent systems for use as building materials.

The multicomponent oxide system $CaO\text{-}SiO_2\text{-}Al_2O_3\text{-}Fe_2O_3\text{-}MgO$ is very important for wide application in various technologies for the production of ceramic, composite, and glassy materials, as well as metallurgy. However, there is currently no data on the structure of multicomponent systems containing more than 3 phase-forming oxides, which requires appropriate research to determine their structure.

The figurative points of some regolith compositions reduced to the corresponding three-component systems with a 100% recalculation of the composition are shown in *Fig. 2* [11-13].

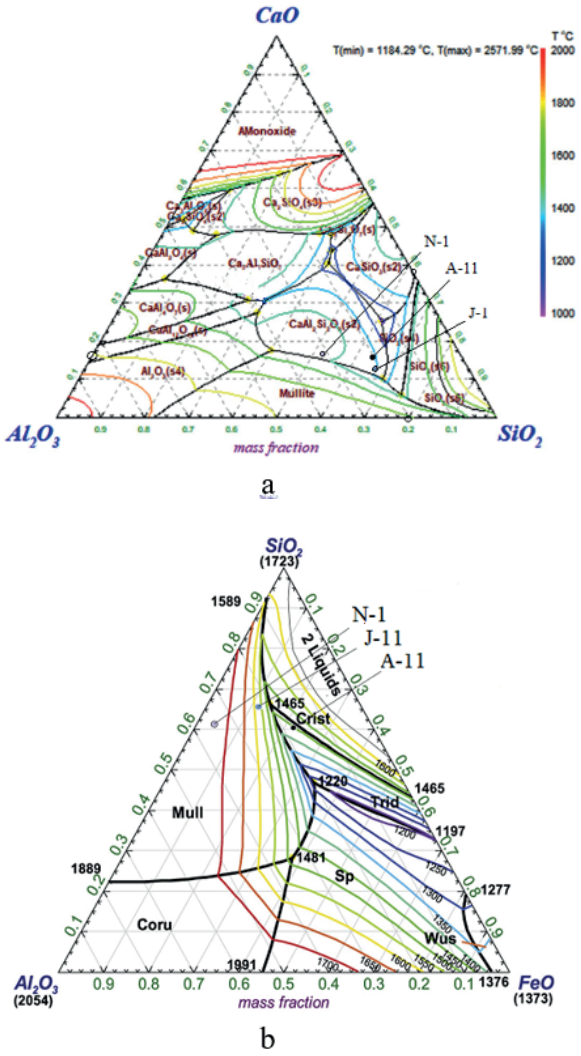

Fig. 2 Three-component oxide systems that are promising for obtaining materials based on regolith a - SiO_2-Al_2O_3-CaO system [11,12], b - SiO_2-Al_2O_3-FeO system [13]

2. ábra Háromkomponensű oxidrendszerek, amelyek ígéretesek regolit alapú anyagok előállítására a – SiO2–Al2O3–CaO rendszer [11,12], b – SiO_2–Al_2O_3–FeO rendszer [13]

A number of articles are planned on this topic related to the fundamental study of promising multicomponent systems for use as building materials in the space industry with the potential for 3D printing and the expansion of the areas of building materials production.

2.2 Properties of regolith

Lunar regolith has several unique physical and chemical properties that distinguish it from Earth's soil. These properties are important for understanding the lunar geology and planning future exploration missions, as well as utilizing its resources.

Regolith consists of very fine dust (often called lunar dust) with particle sizes ranging from submicron to several millimeters. Lunar dust is very abrasive because it is not subject to atmospheric or water weathering, which means that the particles retain sharp edges.

On the surface, regolith has a low bulk density (1.5 g/cm^3), but at deeper levels it becomes denser. The upper layers of regolith are porous, with voids between the particles.

Due to the limited amount of real lunar material, the research was mainly conducted using regolith simulants. The simulants are formulated to mimic lunar soil samples obtained during the Apollo missions (the Apollo program made a manned landing on the Moon and conducted an on-site inspection; ~380 kg of lunar regolith samples, including basalt, breccia, plutonite, soil, core, and other materials, were delivered to Earth for further scientific research [15]).

In addition, lunar regolith is also rich in glass fragments and their agglutinates formed by meteorite impacts. Therefore, basaltic lava or volcanic ash is commonly used as a raw material for lunar regolith simulants, such as JSC-1A and BP-1 in the United States, KLS-1 in Korea, UoM-B&M in the United Kingdom, and DNA-1 in Italy. Widely used simulators in China, such as CAS-1, CLRS-1 and 2, TJ-1, and NEU-1a and b, are also made on the basis of basaltic volcanic soriate [16].

When it comes to practical use in extraterrestrial environments, it is important to evaluate the properties of various building materials and select appropriate materials based on specific construction requirements. These requirements mainly stem from the extreme extraterrestrial conditions that can cause difficulties in both the preparation and application process. Specifically, extreme extraterrestrial conditions include space debris, hard vacuum, low gravity, temperature fluctuations, weak atmosphere, and extreme radiation. Extraterrestrial construction materials must provide a safe and stable environment for astronauts during the construction of extraterrestrial structures. Accordingly, the requirements for the properties of building materials can be divided into three categories: mechanical, thermal, optical, and radiation protection.

2.2.1 Mechanical properties

Almost all samples of extraterrestrial structures were tested for compressive strength. In addition, to determine impact resistance, Allende et al. conducted 19 experiments with high-speed impacts [17]. Analytical power-law relationships were obtained to predict transient crater dimensions such as volume and diameter based on projectile characteristics such as diameter, density, and velocity. The scaling exponents determined for the volume and diameter of transient craters in BSC are comparable to those in quartzite, sandstone, and basalt, indicating that cratering in BSC is largely driven by projectile kinetic energy, as expected for cohesive low-porosity materials.

The nanohardness of samples of molten regolith was investigated by Zheng et al. [18], in which a nanoindenter applied a force of 0.1 N to the sample. The coefficient of thermal expansion ranges from 6.42 × 10^{-6} 1/°C to 9.82 °C × 10^{-6} 1/°C between the initial temperature (30 °C) and the softening temperature (919 °C), and the thermal conductivity and specific heat capacity are close to concrete. At room temperature, the compressive strength and flexural strength are 67.1 ± 31.9 MPa and 100.7 ± 31.3 MPa, respectively, which are much higher than those of traditional cement on Earth. The microhardness of the SPS, DLP, and laser-sintered samples was tested by other researchers using Vivtorinox hardness testers. The fatigue curve of the "lunar cement" was obtained by Su et al. The fatigue resistance of JSC-1a-based IOH is higher than that of typical

steel-reinforced concrete under the same loading conditions, especially when the stress amplitude is relatively high.

Thermal and optical properties of building materials also have a significant impact on determining their suitability for building and life safety.

2.2.2 Thermal properties

The low values of the coefficient of thermal expansion (CTE) of the material obtained by using regolith will make the stresses in the structure arising from the thermal load on it acceptable. Accordingly, Kim et al. studied the coefficient of thermal expansion of regolith samples sintered in a microwave oven [20]. With an increase in sintering temperature, linear shrinkage and density increased, while porosity decreased. Structural changes in the sintered samples were characterized by scanning electron microscopy and X-ray diffraction. Unconfined compression strength tests showed that the mechanical strength increased significantly with increasing sintering temperature, with the highest strength of 37.0 ± 4.8 MPa being achieved at 1120 °C. The sintered samples had a coefficient of thermal expansion of approximately 5×10^{-6} °C-1, which was well preserved even after cyclic temperature loads from -100 to 200 °C.

In addition, good thermal insulation properties and adequate light absorption will allow creating habitable conditions in the room. The diffusive heat capacity and thermal conductivity of various sintered samples were investigated by Fateri et al. [21]. Thermal conductivity measurements showed that the thermal conductivity increases for each individual sample (regardless of the sintering method) by about 10% in the temperature range from 25°C to 150 °C. The laser sintering of JSC-2A showed the highest thermal conductivity of approximately 1.1 Wt/m × K at room temperature compared to the other sintered samples.

2.2.3 Optical properties

The optical properties of regolith powders and corresponding SPS samples were tested by Licheri et al. They compared the optical properties of sintered samples and the original regolith powders, taking into account spectral absorption/emission, integrated solar absorption, and integrated thermal radiation, evaluated in the temperature range representative of ISRU applications, i.e. from 100 to 1300 K. It was found that sintering changes the optical properties of regolith depending on the process, with sintered pellets exhibiting increased solar absorption and thermal emission compared to the original powders [22].

2.2.4 Radiation properties

Radiation protection properties play an important role when considering extreme radiation in outer space. Building materials with good radiation protection properties can support the long-term stay of astronauts in space. Montes et al. [23] conducted a simulation to study the protective properties of geopolymer concrete against proton radiation. Comparison of the modeling results made it possible to independently assess the required level of regolith protection to cope with primary and secondary radiation. For galactic cosmic rays, a value of > 200 g/cm^2 is estimated to result in a >50% reduction in throughput. For solar radiation, several tens of g/cm^2 can reduce the dose by more than an order of magnitude. To protect against neutron radiation, lunar regolith simulator samples were tested by Meurisse [24]. Neutrons were produced in the process of proton splitting with an energy of 800 MeV. The modeling results showed that the mechanical and chemical properties allow for sufficient radiation protection of the crew inside the lunar living quarters without additional requirements. To protect against heavy ions, both lunar regolith and regolith simulators were tested [25]. Measurements and model calculations show that a small amount of lunar soil provides significant protection against primary proton nuclei with solar particle energy, with a small residual dose from surviving charged fragments of heavy rays.

The data from the above studies are a valuable source for determining the preferred types of building materials when they are made from regolith.

2.3 Promising areas for the use of building materials from regolith

Regolith is considered a potential resource for future lunar bases. Extraterrestrial regoliths can serve as primary raw materials for the production of building materials. Through the use of remote sensing and experiments on real samples, a certain understanding of lunar regoliths has been accumulated.

Due to its accessibility, regolith as the main raw material is promising for the construction of extraterrestrial structures. With chemical components similar to those of terrestrial rocks, regolith can be used to make concrete or other composite materials, as well as to produce brick building blocks. In addition, useful chemical components of modified admixtures, such as S and Mg, can be extracted in situ from regolith to reduce the burden of extraterrestrial transportation, and can be directly used as radiation and heat shielding layers in structures, which helps reduce the cost of transporting materials from the Earth [2].

Concrete-like materials have the highest potential for use in extraterrestrial construction due to their natural mechanical properties, stability, and durability. Therefore, building materials that use few resources such as geopolymers while providing sufficient protection against harsh lunar conditions are of interest.

The production of glass from lunar regolith also has a wide range of applications, including substrates for semiconductors, windows, pipes, and other molded objects. Such glass can be used for thermal insulation foams and heat shields, which contributes to the development of lunar infrastructure, including habitat modules and scientific laboratories.

Glass production involves three steps: melting sand, forming hot glass, and heat treatment to prevent cracks. On the Moon, raw materials are limited to basalt sand, so the properties of glass depend on its composition. Basalt glass is formed by melting basalt material and occurs naturally both on Earth (e.g. obsidian) and on the Moon. The content of basalt glass in regolith can affect the production process by reducing the temperature and energy required for melting.

Mirror production on the Moon requires high-quality glass and the application of a reflective material such as aluminum, which is highly reflective (~90%) in the visible spectrum. Silver

is less reflective below 400 nm. To achieve optimal reflective characteristics, an aluminum layer thickness of ~100 nm is required. To produce a mirror surface with an area of 100 m² and a density of 2700 kg/m³, 27 g of aluminum with a purity of 99.999% is required. Taking into account losses, less than 1 kg of high-quality aluminum needs to be purified on Earth and sent to the Moon, which is a viable approach for a lunar mission [26].

Thus, using the material basis provided by extraterrestrial regolith simulators, dozens of methods for preparing regolith-based building materials have been proposed by various researchers. According to the molding principle, building materials can be produced in three main ways: concrete curing, additive manufacturing, and regolith sintering/melting. Concrete materials for extraterrestrial construction mainly include sulfur, biopolymer, geopolymer, polymer, and silicate [27-31].

Compositions of this system are the basis of high alumina and Portland cement, ceramic bricks and tiles, mullite, forsterite, and cordierite refractories, foam glass, and steel production wastes. Understanding the thermodynamics of this system and the complex interactions between these oxides is crucial for its application. Traditionally, this has been done using the well-known binary or ternary diagrams, where the interactions between two or three components are considered simultaneously. However, modern methods of theoretical research allow obtaining information on the susceptibility state of systems that include four components [32].

2.4 Application of additive technologies

With the rise of additive manufacturing (3D printing), complex geometries can be created directly from a computer design file. This process is defined both on Earth (e.g. obsidian) and on the Moon. The content of basalt glass in regolith can affect the production process by reducing the required temperature and energy for melting.

Analysis of research shows that the main extraterrestrial construction processes are carried out by two methods, namely additive manufacturing (3D printing) or prefabrication using sintered regolith bricks. From the perspective of extraterrestrial construction, 3D construction methods have become the most promising because of their environmental friendliness, given the huge economic costs of extraterrestrial transportation. Accordingly, extraterrestrial regolith is the main raw material available. The value of lunar regolith samples prevents the use of destructive experiments for construction research.

3D printing parts for space exploration is not just an Earth-based activity. For years, NASA and other space agencies have been printing polymer parts on the International Space Station.

Initial studies have shown the feasibility of processing lunar simulant powders using various bulk ceramic sintering methods, including traditional sintering, microwave sintering, solar sintering, 3D printing, direct laser production, selective laser melting, and glass formation techniques [2].

The abundance of regolith makes it a promising material for the production of building materials, such as lunar concrete or 3D printed structures for housing.

Several ISRU ("In-Situ Resource Utilization") methods have been proposed in the research, which translates to "in-situ resource utilization". In particular, several techniques involve the creation of concrete and cement materials. The authors of [33] proposed a 3D printing process with Sorel cement (magnesia cement) for construction on the Moon, but this technology required significant amounts of chemicals and water. Researchers [34] have developed a stone-like material using phosphoric acid that is promising for Mars, but not for the Moon, due to the need to transport water and acid.

In [35], the researchers focused on analyzing the properties of NU-LHT-2M that could be most critical for the selective laser melting process. The main focus was on the granulometry and the presence of water in the powder, due to the influence of an uncontrolled atmosphere during previous tests.

To avoid contamination due to the presence of water as much as possible, it was decided to place the batch in a thermal vacuum chamber for 24 hours, after which it was stored in sealed silicone containers. The presence of water proved difficult to completely avoid, but the experiments were not spoiled by the small residues left in the used powder. The second main problem was the grain size present in the batch, which should have been on average 100 μm with maximum values of about 1 mm, while the results obtained with the Malvern Mastersizer 2000 (particle size distribution analysis instrument) showed a slightly offset size of up to 250 μm.

The use of a 250Wt fiber laser at 1070 nm in previous work has shown that it is capable of effectively melting the JSC-1A simulant and producing strong 3D printed objects while operating at approximately 20% of its maximum power. The reflectivity values at the desired wavelength are not sufficiently different to justify the choice of a different laser type, so it was not changed in this work. The chemical composition of the two simulants should be different since they are designed to be similar to the soil of different regions of the Moon, but knowing some of the main components of the powder provides clues to fine-tune the process to improve it [36].

One of the missing information about 3D printing with lunar regolith simulant is the compressive strength of the material, which is introduced in this paper but needs further development to obtain accurate results suitable for the actual construction process with 3D printed lunar dust. In this study, the strength was measured using a strain gauge connected to a hydraulic press that imposed displacement values on a moving head. The material showed brittle behavior, as expected for ceramics, and strength comparable to concrete, reaching medium ultimate stresses.

One of the main advantages of this technology is the ability to print high-quality parts very quickly and without the need for tools. Given the high resolution and relative density of the samples, the ability to produce extremely precise, small and complex porous regolith parts such as catalysts and filters will allow for a significant breakthrough in the long-term space development of mankind.

Building 3D printing has significant potential for building in such harsh environments due to its robotic and autonomous capabilities. NASA is considering this technology for construction outside the world, and in 2015-2019 organized the "3D Printed Environments Competition", which awarded a total of $5 million to teams with construction solutions. In 2020,

NASA's Johnson Space Center 3D printed a 1,700-square-foot environment (Mars Dune Alpha) to simulate the habitat of Mars. To realize an efficient planetary construction process, resources on the Moon and Mars must be used as printing materials. For example, sulfur concrete is an anhydrous alternative material that is well suited for planet construction. Elemental sulfur can be extracted from sulfate-sulfide mineral deposits on the Martian or lunar surface using ISRU technologies.

2.5 Further experiments and research on this topic

Within the framework of this research topic, a series of scientific publications is planned. In the subsequent stages of the study, attention will be focused on the in-depth investigation of multicomponent systems, particularly ternary and quaternary oxide systems such as SiO_2–Al_2O_3–FeO and SiO_2–Al_2O_3–CaO. The primary objective is to explore phase interactions within these systems, conduct thermodynamic modeling, calculate equilibrium phase diagrams, and provide a thermodynamic rationale for the formation of target crystalline phases with desired properties.

Theoretical results obtained from this study will serve as a foundation for the rational selection of material compositions, which will subsequently be synthesized under laboratory experimental conditions. For each selected composition, melting diagrams will be constructed to determine the temperature ranges of phase formation, as well as to establish optimal technological parameters for their synthesis, including heat treatment regimes and cooling conditions.

In addition to traditional ceramic processing methods such as forming and sintering, the developed compositions will be evaluated for their suitability in modern additive manufacturing techniques, particularly 3D prototyping. This approach will enable the assessment of the materials' potential for producing components with complex geometries and their integration into space and advanced construction technologies, taking into account structural integrity, thermal resistance, and functional performance requirements.

These investigations are aimed at establishing a scientific foundation for the development of efficient and energy-viable technologies for the in-situ fabrication of construction elements—directly on the surface of celestial bodies—by utilizing locally available resources.

The expected outcomes are anticipated to hold fundamental significance for materials science, ceramic chemistry, and the engineering of future space infrastructure.

3. Conclusions

The research analysis suggests a construction concept based on the use of in situ resources, given the high cost of extraterrestrial transportation.

In the future, with the development of technology and increased experience in the use of lunar resources, the opportunities for creating sustainable and long-term lunar bases will only increase. This opens up prospects for further exploration of the Moon and other space bodies, as well as for the development of new technologies that can be applied both on Earth and in other space missions.

A critical aspect for space applications is the appropriate technology, especially 3D printing technology, which has advantages such as energy efficiency, automation, design freedom, and reduced production time. This is an ideal solution for the production of lunar and Martian bases, but more efficient production methods from local resources need to be developed and the 3D printing process needs to be optimized.

Thus, extraterrestrial construction based on regolithic materials is quite achievable and promises to open up new horizons for humanity. NASA's program and other missions demonstrate the possibility of creating a permanent human presence on the Moon and Mars. The use of local resources, such as lunar regolith, to produce building materials on site, as well as 3D printing and ISRU technologies, make the construction of lunar and Martian bases a reality.

Geopolymers obtained from local lunar materials are a promising building material for the construction of lunar bases. They have high strength, resistance to extreme lunar conditions, and minimal water requirements, making them an ideal choice for extraterrestrial construction. Geopolymers can be used for direct construction with minimal human involvement, which is critical to eliminate the costly transportation of construction materials and astronaut activities.

Prospects for further development in this area include the development and improvement of technologies for using local resources, such as lunar regolith, to build infrastructure on the Moon. This will reduce the cost of missions, reduce dependence on the transportation of materials from the Earth, and make it possible for people to live on the Moon for a long time. In addition, the development of new technologies, such as additive manufacturing and generative design, opens up new opportunities for creating sustainable and long-term lunar bases.

References

[1] Lucey P. G. et al. (2022) Volatile interactions with the lunar surface. Geochemistry. Vol. 82, No.3, 125858 p. https://doi.org/10.1016/j.chemer.2021.125858

[2] Cheng Zhou, Yuyue Gao, Yan Zhou, Wei She, Yusheng Shi, Lieyun Ding, Changwen Miao (2024): Properties and Characteristics of Regolith-Based Materials for Extraterrestrial Construction. Engineering. Vol. 37, pp. 159-181. https://doi.org/10.1016/j.eng.2023.11.019

[3] Kanamori, H., Udagawa, S., Yoshida, T., Matsumoto, S. and Takagi, K. (1998) Properties of lunar soil simulant manufactured in Japan. Space. Vol. 98, pp. 462–468. https://doi.org/10.1061/40339(206)53

[4] Spray, J.G. (2010) Generation of a lunar regolith agglutinate simulant using friction welding apparatus. Planet. Space Sci. Vol.58, No.14–15, pp. 1771-1774. https://doi.org/10.1016/j.pss.2010.09.002

[5] Carrier W.D. (1973) Lunar soil grain size distribution. The moon. 6(3), pp. 250–263. https://doi.org/10.1007/BF00562206

[6] Heiken G.H., Vaniman D.T., French B.M. (1991) Lunar sourcebook: a user's guide to the Moon Cambridge University Press, Cambridge

[7] Bajpayee A., Farahbakhsh M., Zakira U., Pandey A., Ennab L.A., Rybkowski Z., Dixit M.K., Schwab P.A., Kalantar N., Birgisson B., Banerjee S. (2020) In situ resource utilization and reconfiguration of soils into construction materials for the additive manufacturing of buildings. Front. Mater. Vol. 7, 52 p. https://doi.org/10.3389/fmats.2020.00052

[8] Zheng Y., et al.(2009) CAS-1 lunar soil simulant. Adv. Space Res. Vol. 43, No. 3, 448–454pp. https://doi.org/10.1016/j.asr.2008.07.006

[9] Reiss P., Grill L., Barber S.J. (2019) Thermal extraction of volatiles from the lunar regolith simulant NU-LHT-2M: preparations for in-situ analyses on the moon. Planet Space Sci. Vol. 175, 41-51 pp. https://doi.org/10.1016/j.pss.2019.05.001

[10] Morris RV, Heiken G, Morris R, Score R. (1983) Handbook of lunar soils. Houston: Lyndon B. Johnson Space Center.
[11] Hengbao Ma, Kexin Jiao, Jianliang Zhang, Lei Zhang, Fan Xiaoyue (2020) Phase Composition and Formation Mechanism of Slag Crust in Blast Furnace. ISIJ International. Vol. 60, No.11, 8 p. https://doi.org/10.2355/isijinternational.ISIJINT-2020-113
[12] Haccuria E., Crivits T., Hayes P. C. and Jak: J. E. (2016) Selected Phase Equilibria Studies in the Al_2O_3-CaO-SiO_2 System. Am. Ceram. Soc. Vol. 99, 691 p. https://doi.org/10.1111/jace.13991
[13] Viktoria Prostakova, Denis Shishin, Maksym Shevchenko, Evgueni Jak (2019) Thermodynamic optimization of the Al_2O_3–FeO–Fe_2O_3–SiO_2 oxide system. Calphad. Vol. 67, 101680. https://doi.org/10.1016/j.calphad.2019.101680
[14] Shchukina L.P., Korohodska A.M., Kryvobok R.V., Shabanova G.M. (2024) Small-piece semi-dry-compacted concrete products based on waste from energy generating enterprises. Visnyk NTU «KhPI» 63 S: Khim., khim.tekhn. ta ekol. Vol.2, No 12, pp. 63-70. https://doi.org/10.20998/2079-0821.2024.02.11
[15] Papike J.J., Simon S.B., Laul J.C. (1982) The lunar regolith: chemistry, mineralogy, and petrology. Rev Geophys. Vol. 20, No.4, 761-8267. https://doi.org/10.1029/RG020i004p00761
[16] Ruilin Li, Guoqing Zhou, Kang Yan, Jun Chen, Daqing Chen, Shangyue Cai, PinQiang Mo (2022) Preparation and characterization of a specialized lunar regolith simulant for use in lunar low gravity simulation. International Journal of Mining Science and Technology. Vol. 32, No. 1, pp. 1-15. https://doi.org/10.1016/j.ijmst.2021.09.003
[17] Allende M.I., Davis B.A., Miller J.E., Christiansen E.L., Lepech M.D., Loftus D.J.,(2020) Hypervelocity impact performance of biopolymer-bound soil composites for space construction. J Aerosp Eng. Vol. 33, No.2, 04020001 p. https://doi.org/10.1061/(ASCE)AS.1943-5525.0001110
[18] Zheng W., Qiao G. (2022) Microstructure, thermophysical, and mechanical properties of bulk glass prepared from molten lunar regolith simulant. Adv Space Res. Vol. 69, No.8, pp. 3130-3139. https://doi.org/10.1016/j.asr.2022.01.041
[19] Su H., Hong Y., Chen T., Kou R., Wang M., Zhong Y., et al.(2019) Fatigue behavior of inorganic–organic hybrid lunar cement. Sci Rep. Vol.9, No.1, 2238 p. https://doi.org/10.1038/s41598-019-38799-x
[20] Kim Y.J., Ryu B.H., Jin H., Lee J., Shin H.S. (2021) Microstructural, mechanical, and thermal properties of microwave-sintered KLS-1 lunar regolith simulant. Ceram Int. Vol. 47, No. 19, pp. 26891-26897. https://doi.org/10.1016/j.ceramint.2021.06.098
[21] Fateri M., Sottong R., Kolbe M., Gamer J., Sperl M., Cowley A. (2019) Thermal properties of processed lunar regolith simulant. Int J Appl Ceram Technol. Vol. 16, No. 6, pp. 2419-2428. https://doi.org/10.1111/ijac.13267
[22] Licheri R., Orrù R., Sani E., Dell'Oro A., Cao G. (2022) Spark plasma sintering and optical characterization of lunar regolith simulant. Acta Astronaut. Vol. 201, pp. 64-171. https://doi.org/10.1016/j.actaastro.2022.09.016
[23] Montes C., Broussard K., Gongre M., Simicevic N., Mejia J., Tham J., et al.(2015) Evaluation of lunar regolith geopolymer binder as a radioactive shielding material for space exploration applications. Adv Space Res. Vol. 56, No. 6, pp. 1212-1221. https://doi.org/10.1016/j.asr.2015.05.044
[24] Meurisse A., Cazzaniga C., Frost C., Barnes A., Makaya A., Sperl M. (2020) Neutron radiation shielding with sintered lunar regolith. Radiat Meas. Vol. 132, 106247 p. https://doi.org/10.1016/j.radmeas.2020.106247
[25] Miller J., Taylor L., Zeitlin C., Heilbronn L., Guetersloh S., DiGiuseppe M., et al. (2009) Lunar soil as shielding against space radiation. Radiat Meas. Vol. 44, No. 2, pp. 163-167. https://doi.org/10.1016/j.radmeas.2009.01.010
[26] Schleppi J., Gibbons J., Groetsch A. et al. (2019) Manufacture of glass and mirrors from lunar regolith simulant. J Mater Sci. Vol. 54, pp. 3726–3747. https://doi.org/10.1007/s10853-018-3101-y
[27] Rahim A., Gulzar A., Khan A., Rehman Z. (2021) Mars in situ resource utilization and sulfur concrete. P.J. Van Susante, A.D. Roberts (Eds.), Earth and Space 2021. American Society of Civil Engineers, Reston. pp.1231-1241. https://doi.org/10.1061/9780784483374.114
[28] Rosa I., Coto A., Allende M.I., Lepech M.D., Loftus D.J. (2021) Designing biopolymer-bound regolith composites for maximum compressive strength. P.J. Van Susante, A.D. Roberts (Eds.), Earth and Space 2021, American Society of Civil Engineers, Reston. Vol. 1, pp. 200-214. https://doi.org/10.1061/9780784483381.019
[29] Sakamoto K., Wajima T. (2020) Preparation of geopolymer cement from simulated lunar rock sand using alkali fusion. Int J GEOMATE. Vol. 18, No. 70, pp. 62-67. https://doi.org/10.21660/2020.70.9162
[30] Oh K., Chen T., Kou R., Yi H., Qiao Y.(2020) Ultralow-binder-content thermoplastic composites based on lunar soil simulant. Adv Space Res. Vol. 66, No. 9, pp. 2245-2250. https://doi.org/10.1016/j.asr.2020.07.041
[31] Neves J.M., Ramanathan S., Suraneni P., Grugel R., Radlińska A. (2020) Characterization, mechanical properties, and microstructural development of lunar regolith simulant-portland cement blended mixtures. Constr Build Mater. Vol.258, 120p. https://doi.org/10.1016/j.conbuildmat.2020.120315
[32] Kryvobok R.V., Pitak Y.M., Lisachuk G.V., Voloshchuk V.V., Grebenyuk I.I., Kudii M.O., Bahlai V.Yu. (2024) Spriazheni reaktsii v bahatokomponentnii systemi SrO–BaO–Al_2O_3–SiO_2. Voprosy khimii i khimicheskoi tekhnologii. Vol. 5, pp. 138-145. https://doi.org/10.32434/0321-4095-2024-156-5-138-145
[33] Cesaretti G., Dini E., De Kestelier X., Colla V., and Pambaguian L. (2014) Building components for an outpost on the Lunar soil by means of a novel 3D printing technology. Acta Astronaut. Vol. 93, pp. 430–450. https://doi.org/10.1016/j.actaastro.2013.07.034
[34] Buchner C, Pawelke RH, Schlauf T, Reissner A, Makaya A (2018) A new planetary structure fabrication process using phosphoric acid. Acta Astronaut. Vol. 143, pp. 272–284. https://doi.org/10.1016/j.actaastro.2017.11.045
[35] Reiss P., Grill L., Barber S.J. (2019) Thermal extraction of volatiles from the lunar regolith simulant NU-LHT-2M: preparations for in-situ analyses on the moon. Planet Space Sci. Vol. 175, pp. 41-51. https://doi.org/10.1016/j.pss.2019.05.001
[36] Ray C.S., Reis S.T., Sen S., O'Dell J.S.(2010) JSC-1A lunar soil simulant: characterization, glass formation, and selected glass properties. J Non-Cryst Solids. Vol 356, No. 44–49, pp. 2369-2374. https://doi.org/10.1016/j.jnoncrysol.2010.04.049

Ref.:
Kryvobok, R. V. – **Lisachuk**, G. V. – **Fedorenko**, O. Y. – **Tymchenko**, O. R. – **Riabinin**, O. S. – **Voloshchuk**, V. V. – **Permiakov**, K. Yu. – **Kudii**, D. A. – **Humennyi**, I. I: *Review article: Prospects for creating building materials based on regolith*
Építőanyag – Journal of Silicate Based and Composite Materials, Vol. 77, No. 2 (2025), 32–38 p.
https://doi.org/10.14382/epitoanyag-jsbcm.2025.5

Predicting 28-day compressive and flexural strengths of ironstone concrete using Gene Expression Programming (GEP)

Ugochukwu David NWAKONOBI ▪ Civil Engineering Department, Joseph Sarwuan Tarka University, Nigeria ▪ davidvlingz@gmail.com
M. E. ONYIA ▪ Civil Engineering Department, University of Nigeria, ▪ michael.onyia@unn.edu.ng
O. G. OYESANYA ▪ Civil Engineering Department, University of Nigeria ▪ gabriel.oyesanya@unn.edu.ng
Érkezett: 2025. 04. 30. ▪ Received: 30. 04. 2025. ▪ https://doi.org/10.14382/epitoanyag-jsbcm.2025.6

Abstract
The research investigated the structural performance of concrete made with ironstone as coarse aggregate. Ironstone is available in abundance in the south-eastern part of Nigeria especially Anambra and Enugu states. In view of the usual errors associated with traditional laboratory experimental procedures, a machine learning approach (Gene Expression Programming) was employed in GeneXpro Tools for the prediction of the compressive and flexural strengths of ironstone concrete. For this purpose, a database consisting of 352 data points was constructed by replacing ironstone with granite chippings and river gravel up to 50% in 1:2:4 concrete at 0.45, 0.5, and 0.55 water to cement ratios (W/C) respectively. The data set was divided into two sets called the training and validation datasets having 70% and 30% of the data respectively. The training data set was used to train the algorithm while the validation data set was used to validate the algorithm. The algorithm accuracy was checked by calculating the six commonly used errors: mean squared error (MSE), root mean squared error (RMSE), mean absolute error (MAE), and relatively root squared error (RRSE), coefficient of correlation (R) and R^2 for both data sets. The statistical evaluation shows that the R^2 Values are within range specified in the literature (greater than 0.8 and less than 1.0). At 50% replacement with granite chippings at 0.45W/C, optimum results yielding compressive strength of 32.30 N/mm^2 and flexural strength of 13.15 N/mm^2 was achieved. The accuracy of the algorithm was verified using K-Fold cross validation, plotting scatter and shapely sensitivity test. Thus the developed equation can be used to forecast the 28-day compressive and flexural strengths of ironstone concrete.
Keywords: Ironstone concrete, compressive and flexural strengths, modelling, machine learning, gene expression programming
Kulcsszavak: vasércbeton, nyomószilárdság és hajlítószilárdság, modellezés, gépi tanulás, génexpressziós programozás

David Ugochukwu NWAKONOBI
is a Lecturer in the Department of Civil Engineering, Joseph Sarwuan Tarka University, Makurdi, Nigeria. He holds a B.Eng. in Civil Engineering and an M.Eng. in Structural Engineering from the University of Nigeria, Nsukka. His research focuses on the application of Artificial Intelligence and Machine Learning techniques, particularly Gene Expression Programming (GEP), for optimizing concrete and structural performance. He is a registered member of COREN and the Nigerian Society of Engineers (NSE), with professional experience in structural design, project management, and advanced materials research.

Mike ONYIA
is a Professor of Civil Engineering at the University of Nigeria, Nsukka. He holds B.Eng. and Ph.D. degrees in Civil Engineering from the University of Nigeria, and an M.Eng. from Enugu State University of Science and Technology. His research interests span structural and geotechnical engineering, with over 100 peer-reviewed publications in reputable journals. He has held notable positions including Head of the Department of Civil Engineering, General Manager/Chief Executive of ENSEPA, and Non-Executive Commissioner at the Nigerian Communications Commission. Prof. Onyia is a registered engineer with COREN and a corporate member of the Nigerian Society of Engineers.

Gabriel Oluwatosin OYESANYA
is a structural engineer and academic researcher with expertise in structural analysis and sustainable construction materials. He holds an M.Sc. in Civil Engineering from the University of Ibadan and a B.Eng. in Civil Engineering from the University of Nigeria, Nsukka. His research focuses on the development and characterization of alternative aggregates, optimization of concrete performance, and the advancement of environmentally friendly construction technologies. He has professional experience in both academic and industrial settings and is committed to promoting innovative approaches to structural design and materials engineering.

1. Introduction

Ironstone, a sedimentary rock with a high iron content, has traditionally been valued in the construction industry for its strength and durability. Due to its mineral composition, which typically includes iron oxides and silica, ironstone has the potential to improve the mechanical properties of concrete when used as an aggregate. This unique material is becoming an increasingly attractive alternative in concrete production, especially as researchers explore sustainable materials that can enhance the durability and strength of concrete. Ironstone's composition varies based on its geographic source, but it generally contains significant amounts of iron oxide, silica, and sometimes calcium carbonate. The high iron content can contribute to the concrete's compressive strength, especially in structural applications where load-bearing capabilities are essential [1]. Additionally, ironstone's durability and resistance to weathering make it suitable for environments that experience harsh climatic conditions [2].

However, the use of ironstone in concrete also comes with challenges. Its dense nature and high iron content can affect the workability of the concrete mix, potentially requiring the addition of plasticizers or other admixtures to achieve the desired consistency [3]. Despite this, the material has shown promise in studies exploring its use in concrete. Ironstone aggregates have been found to improve various mechanical properties of concrete, particularly compressive and tensile strength. Studies indicate that the high density and hardness of ironstone contribute to a stronger interfacial bond with the cement matrix. In a study by [4], concrete containing ironstone aggregates demonstrated a 20% increase in compressive strength compared to concrete with traditional limestone aggregates. The researchers attributed this improvement to the ironstone's mineral composition, which enhances the bonding at the aggregate-cement interface. Additionally, ironstone's resistance to chemical attacks, such as sulphate and chloride ion penetration, makes it a suitable choice for concrete used in corrosive environments. This is particularly

important in infrastructure exposed to marine or industrial settings, where durability is a critical concern [5]. However, due to its dark colour, ironstone may retain heat, which could impact concrete's thermal behaviour. This can be mitigated by adjusting the mix design and incorporating other materials to control temperature fluctuations.

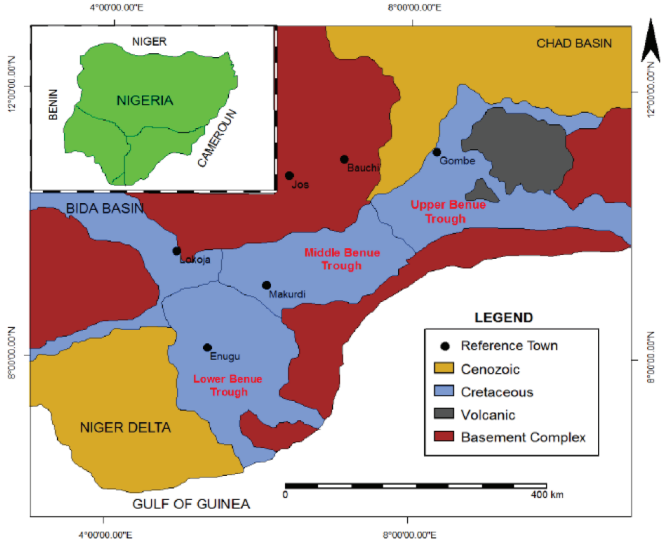

Fig. 1 Geological map of Nigeria showing the location of ironstone (sedimentary) deposit [6]
1. ábra Nigéria földtani térképe, amely a vasérc (üledékes) lelőhelyének elhelyezkedését mutatja [6]

The use of ironstone as an aggregate in concrete aligns with sustainable construction practices, as it utilizes locally sourced materials and can reduce the demand for traditional aggregates like granite and limestone. Research on sustainability in concrete production emphasizes the need to incorporate alternative materials that minimize environmental impact and promote the efficient use of resources [7]. Ironstone's availability in certain regions, especially where iron ore mining is prevalent, makes it a viable option for local sourcing and reducing transportation-related carbon emissions. Ironstone waste from mining operations can also be repurposed in concrete production. Recycling this material helps to reduce waste, contributing to a circular economy and decreasing the environmental footprint of concrete manufacturing. Studies indicate that ironstone fines can also enhance concrete's packing density, which can lead to a reduction in cement content without compromising strength [8]. Concrete produced with ironstone aggregates is suited for high-strength applications, such as foundations, bridges, and marine structures. Its resistance to environmental stressors makes it ideal for use in areas where durability is essential. However, certain limitations must be addressed to fully utilize ironstone's potential. For instance, the high density of ironstone can increase the overall weight of concrete, which may not be desirable for all applications [9]. Additionally, the need for admixtures to maintain workability can slightly increase costs, though this is often offset by the improved durability and strength of the final product. With advancements in concrete technology and mix design, there is potential for ironstone to play a more significant role in concrete production.

Finally, several studies, including [10] as well as [11], have demonstrated GEP's superior performance in predicting concrete strength compared to traditional ML techniques. [10] applied GEP to predict compressive strength and found that it outperformed other methods like ANNs and SVMs in terms of both prediction accuracy and model interpretability. The development of machine learning models, such as Gene Expression Programming (GEP), can aid in optimizing mix designs that incorporate ironstone, enabling more efficient use of this material and enhancing performance outcomes [12]. Future research should focus on exploring ironstone's long-term effects on concrete properties, particularly in diverse environmental conditions. Ironstone presents a promising alternative aggregate for concrete production, offering enhanced strength and durability. While there are challenges related to workability and density, these can be addressed through proper mix design and the use of admixtures. The sustainable aspects of using ironstone, such as local sourcing and waste reduction, further enhance its viability.

1.1 Gene expression Programming (GEP)

It has become clear that algorithms are helpful tools for reducing building waste and encouraging the use of locally abundant materials. According to [13], Gene expression programming (GEP) is a computational technique inspired by biological evolution and genetics. It is used in computer science and machine learning to evolve computer programs that solve specific problems [14]. In GEP, a population of computer programs (represented as strings of symbols) undergoes evolution through processes like mutation, crossover, and selection, similar to natural selection in biology. After which the effectiveness of these initiatives in resolving the issue at hand is assessed. GEP is a cutting-edge artificial intelligence (AI) method that makes use of evolutionary algorithms, according to [15]. It is based on Darwin's theory of natural selection and is a subtype of genetic programming (GP). A set of functions is used by GEP to generate a mathematical expression called a chromosome, which contains numerous genes [16]. A computer program is created by combining the genes that are produced by combining these functions in various ways. Many generations are needed to acquire the necessary fitness before this chromosomal creation process is completed. Individuals in the GEP are expressed as non-linear entities with varying sizes and forms (expression trees) after being encoded as symbolic strings with a fixed length (chromosomes). Because of this difference, GEP may effectively pass the phenotypic threshold and conduct unrestricted search space exploration, opening up new vistas. Furthermore, when compared to other genetic algorithms, GEP performs noticeably better because to its intricate translation mechanism between genotype (chromosomes) and phenotype (expression trees) [17]. Symbolic regression, classification, and optimization issues are just a few of the applications that employ GEP's ability to automatically identify intricate relationships and patterns in data.

1.1.2 Key features of GEP

1. Chromosome Representation: Answers are stored as fixed-length liner strings, or chromosomes.
2. Expression Trees: These depict the functional form of the solution and are translated from the liner chromosomes.
3. Genetic Operators: To evolve the population of solutions over generations, the algorithm uses genetic operators such as mutation, crossover and recombination.
4. Fitness Evaluation: A fitness function that gauges an individual's problem-solving ability is used to assess each member of the population.

For a model to be reliable, it should have R value greater than 0.8 and minimum value of other error metrics such as MAE and RMSE [17]. MAE measures the average deviation between actual and predicted values whereas RMSE indicates the presence of large errors. The errors are squared before taking mean in RMSE, so it gives more weight to larger errors. Its value is always greater than MAE. A model with high RMSE implies that the percentage of predictions with larger errors is greater and should be minimized [18]. The performance index offers the advantage of considering the values of relative root mean square error (RRMSE) and R simultaneously. Its values range from zero to infinity and the model will be reliable if its value is less than 0.2.

Fig. 2 Manually crushed and deposited ironstone [19]
2. ábra Kézzel zúzott és deponált vasérc [19]

2. Methods and material

2.1 Materials

Manually crushed and graded (18 mm – 25 mm) ironstone was obtained from Awba-Ofemili in Awka-North local government area of Anambra state (Latitude 6.8810°N and Longitude 7.5440°E), Nigeria. Crushed granite and the river gravel used were obtained from Gboko in Gboko local government area of Benue State (Latitude 7.8664°N and Longitude 7.9911°E), Nigeria. Sharp sand was obtained at Agu-Opi in Nsukka local government area of Enugu State (Latitude 7.8664°N and Longitude 7.9991°E), Nigeria. Portland cement manufactured by BUA International Ltd (CEM 1 AND 11; 42.5N) in accordance with BS EN 197-1 specification was used. The Portland cement was procured from the building material market in Nsukka community of Enugu State. The water used was supplied by the civil engineering laboratory system in the University of Nigeria, Nsukka, Enugu State, Nigeria. It was clean and free from deleterious materials and meets the requirements of ASTMC1602.

2.2 Method

2.2.1 Compressive strength test

The compressive strength of the hardened concrete cubes was determined in accordance with [20] using a 30 kN capacity electro-hydraulic testing machine in the UNN Civil Engineering Laboratory. Each specimen was loaded gradually until failure, and the maximum load at failure was recorded. The compressive strength was calculated as

$$fcs = \frac{P}{A}$$

Where F is the compressive strength, P is the maximum applied load to the specimen (in Newton, N) and A the cross sectional area of the specimen (in square millimetres mm^2). The average compressive strength of each batch was then computed.

2.2.2 Flexural strength test

Flexural strength was assessed following [21] using simply supported concrete beams (450 × 100 × 100 mm) tested under third-point loading on a universal testing machine. Failure occurred in tension at the bottom fiber, and the flexural strength was calculated as

$$ffs = \frac{FL}{bd^2}$$

where F is the maximum applied load (N), L is the span length (mm), and b and d are the breadth and depth of the beam, respectively.

2.2.3 Concrete mix design

The mix design followed the British Department of Environment (DOE) method (1975, revised 1988) with a target strength of 35 MPa at 28 days and a maximum aggregate size of 20 mm. The concrete was unreinforced, with coarse aggregates comprising ironstone, granite chippings, and river gravel. A water–cement ratio of 0.50 was adopted to achieve the desired strength.

Based on the design procedure, the final mix per cubic meter consisted of 360 kg cement, 621.2 kg fine aggregate, 1320 kg coarse aggregate, and 163.6 kg water. This composition ensured the required strength, acceptable workability (50 mm slump), and conformity with academic and industry standards.

2.2.4 Gene expression programming (GEP)

Gene Expression Programming (GEP) was used in this study to model the nonlinear relationship between concrete mix components and mechanical performance. The method was chosen for its ability to automatically generate predictive equations without predefined assumptions, unlike traditional empirical approaches. Using experimental data, the input variables were water, cement, sand, ironstone, granite chippings, and river gravel, while the outputs were the 28-day compressive strength and flexural strength. Through iterative cycles of chromosome generation, mutation, recombination, and selection, GEP evolved mathematical expressions capable of accurately predicting strength from the given mix parameters.

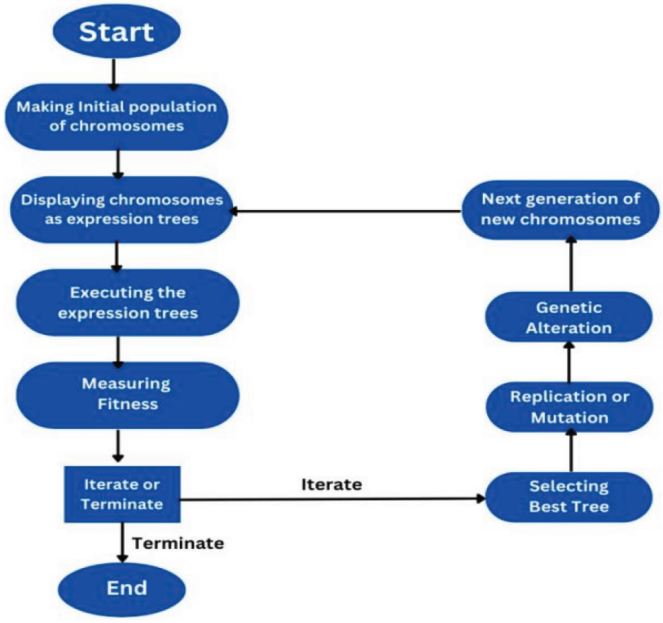

Fig. 3 Gene Expression Programming flowchart [22]
3. ábra Génexpressziós programozás folyamatábrája [22]

The GEP algorithm was implemented using a software known as GeneXpro Tools. The linking function used for the GEP model development was addition alongside other mathematical operations. The final parameters used in algorithm development are shown below in *Table 1*.

Parameter	Settings
Number of Chromosomes	30
Number of Genes	6
Head Size	8
Linking Function	Addition
Constants per Gene	10
Data Category	Floating
Lower and Upper Limit	- 10 to 10
Functions	+, -, ×, /, sqrt, cbrt, exp, ln, invrs
Training Records	687
Validation/Test Records	343

Table 1 Parameters of GEP Model.
1. táblázat A GEP modell paraméterei

2.2.3.1 Performance evaluation

The accuracy and effectiveness of the developed model was evaluated using the following five commonly utilized error metrics:

$$\text{Mean squared error (MSE)} = \frac{1}{n}\sum_{i=1}^{n} (t_i - O_i)^2$$

$$\text{Relative root squared error (RRSE)} = \sqrt{\frac{\sum_{i=1}^{n} (y_i - \hat{y}_i)^2}{\sum_{i=1}^{n} (y_i - \underline{y})^2}}$$

$$\text{Root mean squared error (RMSE)} = \sqrt{\frac{1}{n}\sum_{i=1}^{n} (t_i - O_i)^2}$$

$$\text{Mean absolute error (MAE)} = \frac{1}{n}\sum_{i=1}^{n} (y_i - \hat{y}_i)$$

$$\text{Coeff. Of correlation (R)} = \frac{\sum_{i=1}^{n} (y_i - \underline{y})(\hat{y}_i - \underline{\hat{y}})}{\sqrt{\sum_{i=1}^{n} (\hat{y}_i - \underline{\hat{y}})^2 \sum_{i=1}^{n} (y_i - \underline{y})^2}}$$

3. Results and discussion

This section presents and interprets the results obtained from the experimental investigation and predictive modeling of the concrete mixes.

Replacements (%)	28 Days					
	Compressive Strength (N/mm²)			Flexural Strength (N/mm²)		
	0.45W/C	0.5W/C	0.55W/C	0.45W/C	0.5W/C	0.55W/C
0%I 100%G 0%R	37.98	34.65	33.00	15.55	12.32	10.15
0%I 0%G 100%R	33.80	32.88	30.88	10.89	8.88	7.81
90%I 10%G 0%R	19.15	19.11	16.58	4.95	3.81	2.35
80%I 20%G 0%R	18.17	17.79	16.45	4.69	3.44	2.70
70%I 30%G 0%R	17.96	17.94	16.56	5.53	5.18	5.18
60%I 40%G 0%R	18.97	17.94	17.81	7.20	6.92	5.75
50%I 50%G 0%R	32.30	27.04	22.38	13.15	10.79	7.30
90%I 0%G 10%R	15.86	15.38	14.01	3.99	2.35	2.23
80%I 0%G 20%R	15.32	14.90	13.56	4.12	3.10	2.37
70%I 0%G 30%R	15.50	16.50	15.38	4.28	4.99	4.25
60%I 0%G 40%R	21.93	19.81	17.02	6.98	6.79	5.50
50%I 0%G 50%R	28.11	21.00	22.02	9.87	8.34	7.30
90%I 5%G 5%R	18.69	21.00	17.10	3.10	2.93	2.45
80%I 5%G 15%R	16.31	15.89	15.10	3.42	3.15	2.78
70%I 5%G 25%R	17.77	15.99	15.78	5.10	4.85	5.08
60%I 5%G 35%R	18.64	17.67	17.51	5.99	5.99	6.69
50%I 5%G 45%R	22.31	20.32	20.51	8.51	8.10	7.95
80%I 15%G 5%R	18.32	17.10	15.19	3.18	2.40	3.51
70%I 25%G 5%R	19.11	16.93	15.98	5.32	4.85	4.52
60%I 35%G 5%R	22.45	21.33	17.65	7.41	6.82	5.45
50%I 45%G 5%R	30.04	25.22	20.15	12.50	10.85	9.12
100%I 0%G 0%R	17.50	16.54	14.30	4.52	2.94	2.18

Hint: I=Ironstone, G= Granite, R=River-gravel

Table 2 Average Compressive strength and Flexural strength tests results at 0.45W/C, 0.5 W/C, 0.55W/C. (values represent the arithmetic mean of three specimens)
2. táblázat Átlagos nyomószilárdság- és hajlítószilárdság-vizsgálati eredmények 0,45 W/C, 0,5 W/C, 0,55 W/C arány mellett. (Az értékek három próbatest számtani átlagát jelentik.)

3.1 Experimental results

To obtain the reported values, the compressive strength for each mix was determined from three cube specimens, and the arithmetic mean was calculated. The same approach was applied to flexural strength, ensuring that *Table 2* reflects average values rather than individual test results. In *Table 2*, at a 50% replacement level with granite chippings and a 0.45 water–cement ratio, the concrete achieved a compressive strength of 32.30 N/mm² and a flexural strength of 13.15 N/mm² at 28 days. In comparison, the control mix without granite chippings at the same W/C ratio recorded 22.38 N/mm² compressive strength and 7.30 N/mm² flexural strength. These results indicate that the inclusion of granite chippings significantly enhanced both compressive and flexural strength, likely due to their higher hardness and better interlocking properties compared to the control aggregates.

3.2 Statistical analysis

The statistical analysis comparing the predicted and experimental outcomes for the 28-day compressive and flexural strengths of ironstone concrete using GEP models is represented. The different errors, including Mean Squared Error (MSE), Relative Root Squared Error (RRSE), R-squared (R^2), Root Mean Squared Error (RMSE), and Mean Absolute Error (MAE), are detailed in *Tables 3* and *4*.

3.2.2 Scatter plots

The scatter plots displaying the comparison between the predicted and experimental values for the GEP model's training and testing of 28-day compressive and flexural strengths, are shown in *Fig. 4* and *5*;

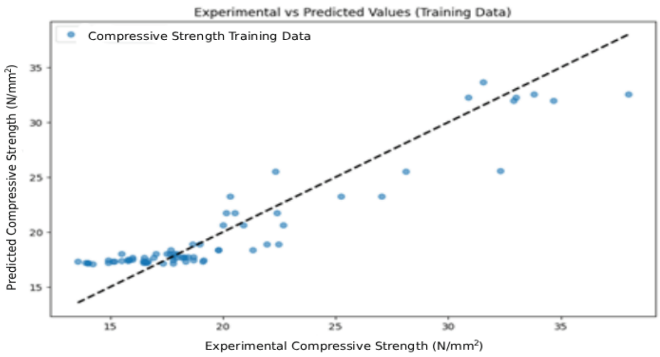

Predicted vs Experimental Values (Training Data)

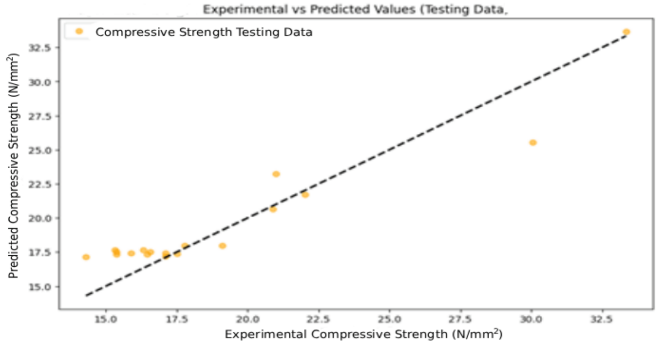

Predicted vs Experimental Values (Testing Data)

Fig. 4 Scatter plots for both Training and Testing for 28 – days Compressive Strength
4. ábra Szórásdiagramok a 28 napos nyomószilárdság tanítási és tesztelési eredményeihez

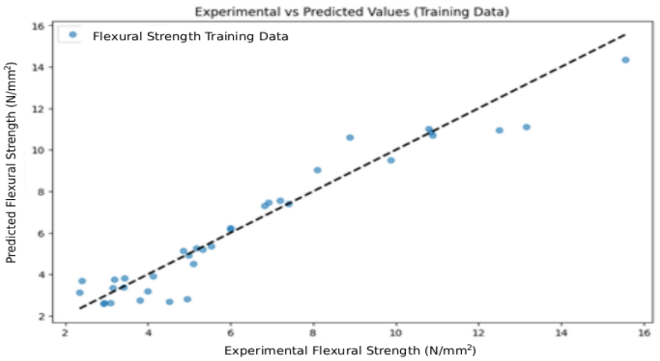

Predicted vs Experimental Values (Testing Data)

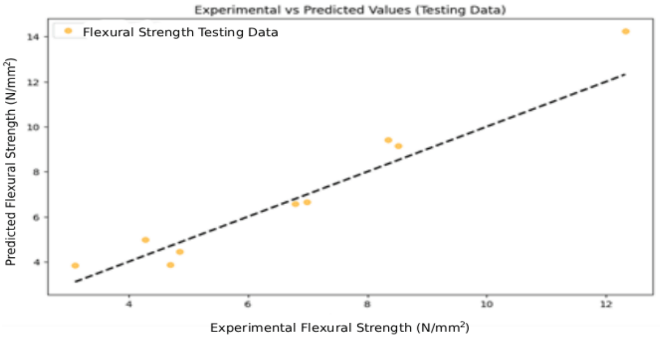

Fig. 5 Scatter plots for both Training and Testing for 28 – days Flexural Strength
5. ábra Szórásdiagramok a 28 napos hajlítószilárdság tanítási és tesztelési eredményeihez

3.2.3 Performance metrics

To evaluate the model's performance, we analysed several metrics: Mean Squared Error (MSE), Relative Root Squared Error (RRSE), R-squared (R^2), Root Mean Squared Error (RMSE), and Mean Absolute Error (MAE) for both training and validation sets for the compressive and flexural strength of various mixtures of concrete made with the aggregates (ironstone) using GEP. The results are shown in *Table 8–9* below.

Description	28 – days	
	Training	Validation
MSE	2.139	4.608
RMSE	1.463	2.147
MAE	1.079	1.405
RRSE	0.243	0.510
Correlation	0.970	0.926
R-Square	0.941	0.858
Best Fitness	406.077	317.81
Max Fitness	1000	1000

Table 3 Performance metrics for 28 days compressive strength.
3. táblázat Teljesítménymutatók a 28 napos nyomószilárdságra

The model for compressive strength shows strong performance on the training data with high R-Square of 0.974, 0.958, 0.94. Low MSE, RMSE, and MAE reflect minimal errors and precise predictions, while a very low RRSE underscores its superiority over a simple mean model in capturing data variability. However, validation metrics reveal challenges: a lower R-Square suggests reduced generalization, and higher MSE, RMSE, MAE, and RRSE indicate larger errors and decreased performance on unseen data, highlighting the need for model refinement to enhance robustness across diverse datasets.

Description	Training	Validation
MSE	0.37492654333821	0.2345183629688
RMSE	0.61231245564517	0.48427096027823
MAE	0.49275211756318	0.40005377626368
RRSE	0.1774017225576	0.27245396561304
Correlation	0.98413929700399	0.97566600817749
R-Square	0.968530153907514	0.951924159513003
Best Fitness	620.227175259184	673.73143230704
Max Fitness	1000	1000

Table 4 Performance metrics for 28 days flexural strength
4. táblázat Teljesítménymutatók a 28 napos hajlítószilárdságra

3.3 GEP expression tree

The hierarchical structure used to represent the mathematical expressions for predicting the 7-, 14- and 28-days compressive strength and the 28 days flexural strength is shown below. It consists of nodes and branches where each node represents an operator or operand, and branches connect nodes to form a complete expression or program (*Fig. 6* and *7*).

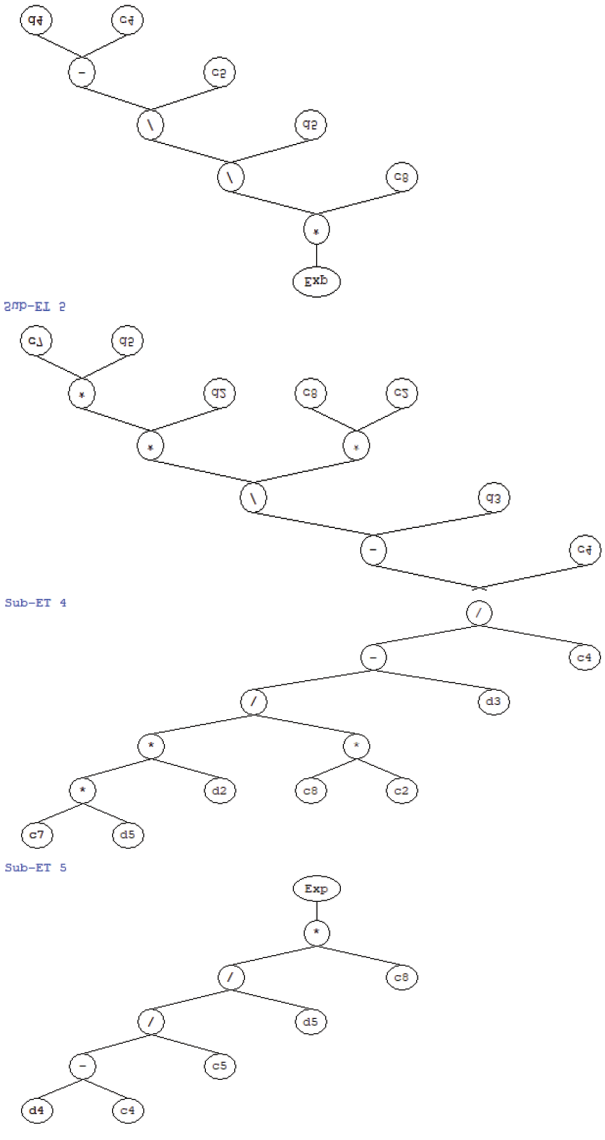

Fig. 6 Expression tree for 28 days compressive strength
6. ábra A 28 napos nyomószilárdság kifejezési fája

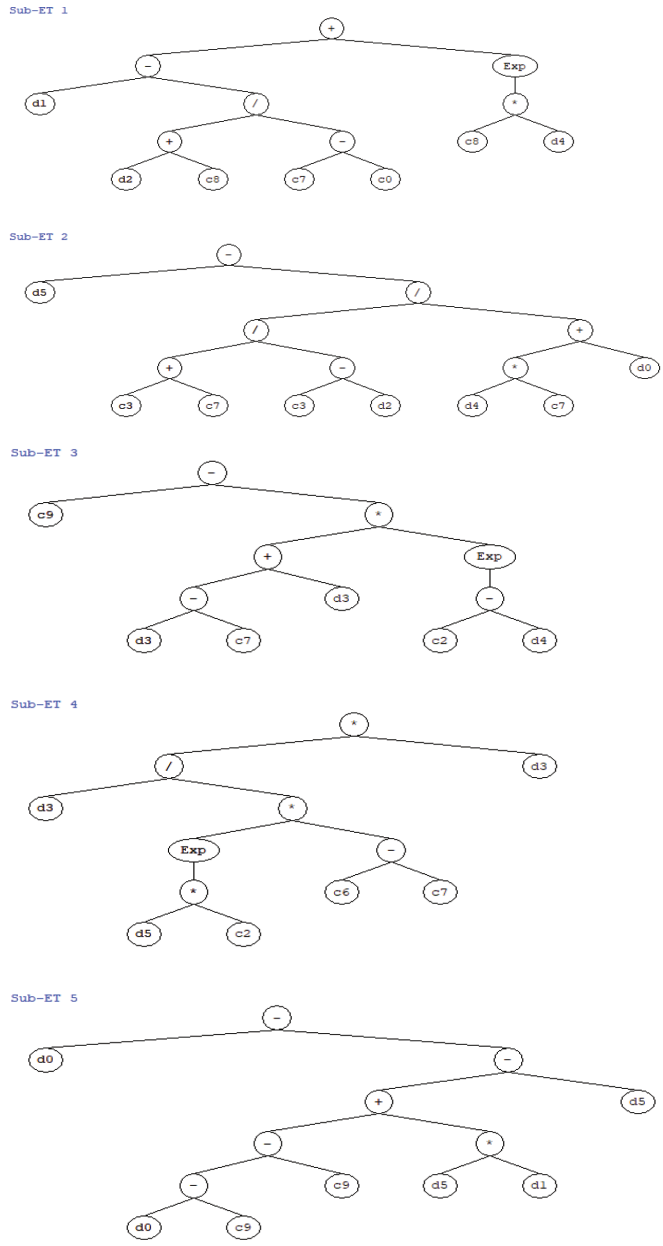

Fig. 7 Expression tree for 28 days flexural strength
7. ábra A 28 napos hajlítószilárdság kifejezési fája

3.3.1 GEP generated equations

The mathematical equations derived from the expression trees described above are crucial for predicting the compressive strength at 28 days, as well as the flexural strength at 28 days. These equations encapsulate the complex relationships between concrete constituents – cement, water, sand, ironstone, granite chippings, and river gravel, providing a structured framework to forecast these critical properties over different time period. The most crucial step in developing a GEP model is determining which parameters have the greatest influence on the final product. To achieve this, a comprehensive analysis was conducted, and multiple trial runs were made in order to determine the most important factors. The GEP method produces an equation that depends on the input parameters listed below.

$f_{Cs} = (d_0, d_1, d_2, d_3, d_4, d_5, c_0, c_2, c_4, c_5, c_6, c_7, c_8, c_9)$

where f_{Cs} is a function of the input parameters of compressive strength for the resulting equations from the GEP algorithm, $d_0, d_1, d_2, d_3, d_4, d_5$ are water, cement, sand, ironstone, granite chippings and river gravel while $c_0, c_2, c_3, c_6, c_7, c_8, c_9$ are strength, 28day strength, 0.45W/C, 0.5W/C, 0.55W/C, 28 day respectively.

$f_{fs} = (d_0, d_1, d_2, d_3, d_4, d_5, c_0, c_2, c_3, c_6, c_7, c_8, c_9)$

where is a function of the input parameters of flexural strength for the resulting equations from the GEP algorithm, are water, cement, sand, ironstone, granite chippings and river gravel while are 28 day strength, 0.45W/C, 0.5W/C, 0.55W/C, and 28 day respectively.

The expression tree provided by the GEP technique is shown in *Fig. 6* and *7*, and it is decoded to yield the mathematical equation for the compressive strength of 28 day and flexural strength estimate of 28 day as well. The resultant equations are provided below;

$f_{Cs} = (A + B + C + D + E)$

$f_{fs} = (A + B + C + D + E)$

3.3.2 Compressive Strength GEP Equations (28 Days)

$$A = exp\left[\frac{\left[\frac{\left(\frac{d_2}{c_6}\right)-(d_2-d_1)}{d_5 \times c_0}\right]}{d_0}\right]$$

$$B = d_1 + \left[\frac{exp\left(\frac{d_5}{d_5}\right)}{(d_1-c_2)(d_0-d_3)}\right]$$

$$C = exp\left[\left(\frac{d_2}{(c_9-d_4)}\right) - \left[\left(\frac{d_3}{d_0}\right) + (c_2 \times c_9)\right]\right]$$

$$D = \frac{\left(\left(\frac{d_2(c_7 \times d_5)}{(c_8 \times c_2)}\right)-d_3\right)}{c_4}$$

$$E = exp\left[c_8\left[\frac{\left[\frac{(d_4-c_4)}{c_5}\right]}{d_5}\right]\right]$$

3.3.3 Flexural Strength GEP Equations (28 Day)

$$A = \left[d_1 - \left(\frac{(d_2+c_8)}{c_7-c_0}\right)\right] + (exp(c_8 \times d_4))$$

$$B = d_5 - \left[\frac{\left(\frac{(c_3+c_7)}{(c_3-d_2)}\right)}{(d_4-c_7)+d_0}\right]$$

$$C = c_9 - [((d_3 - c_7) + d_3)(exp(c_2 - d_4)]$$

$$D = d_3\left[\frac{d_3}{(exp(d_5 \times c_2))(c_6-c_7)}\right]$$

$$E = d_0 - ((d_0 - c_9) - c_9 + (d_5 \times d_1) - d_5)$$

3.3.4 K-FOLD cross-validation

The model's reliability for predicting 28-day compressive strength, as well as 28-day flexural strength, was assessed using the k-fold cross-validation method. This method involves randomly partitioning the data into ten groups, using nine for training and one for validation in each iteration. The entire process is repeated ten times to derive an average performance measure. This rigorous k-fold cross-validation procedure ensures that the models achieve high accuracy. Furthermore, comprehensive statistical evaluations including MAE, MSE, RMSE, RRSE, and R-square were conducted and are depicted in *Fig. 8* and *9*. The models' predictive capabilities were further analysed through statistical calculations, as detailed in the equations below.

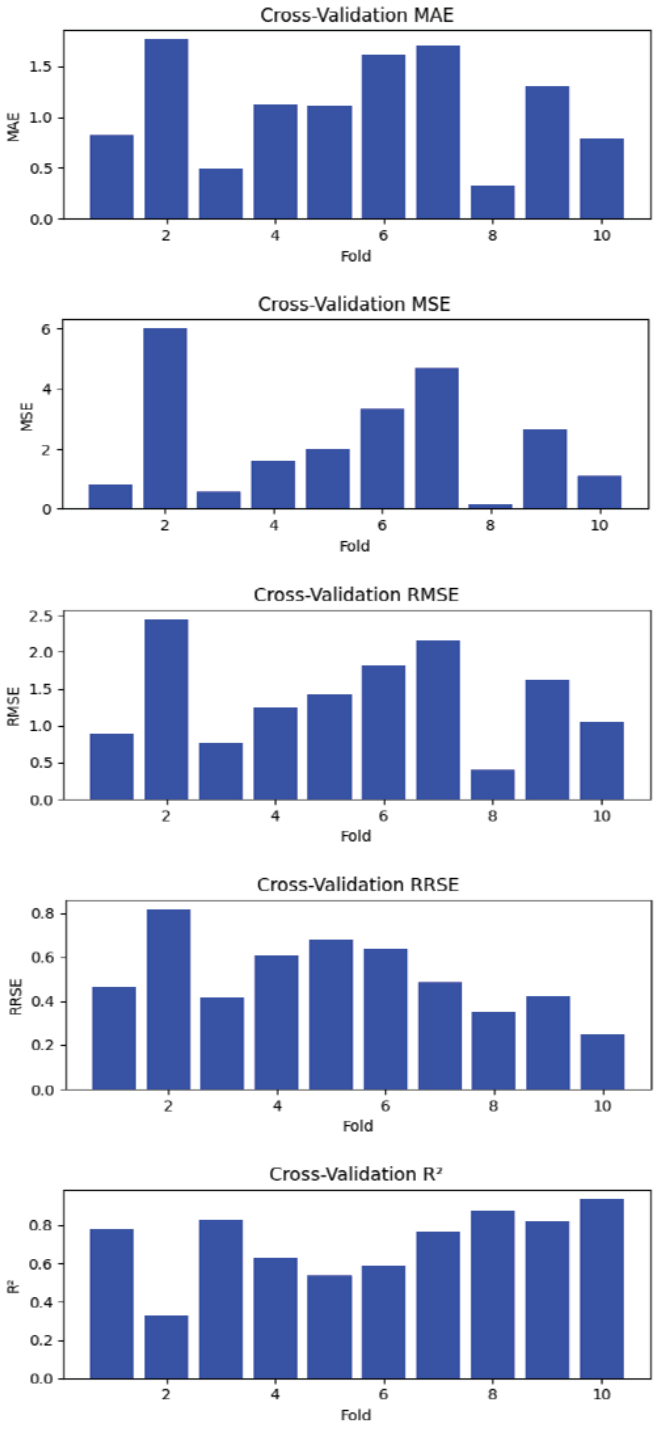

Fig. 8 *28 day Compressive Strength K-fold cross validation for MAE, MSE, RMSE, RRSE and R-square*

8. ábra *A 28 napos nyomószilárdság K-szörös keresztvalidációja MAE, MSE, RMSE, RRSE és R-négyzet értékekre*

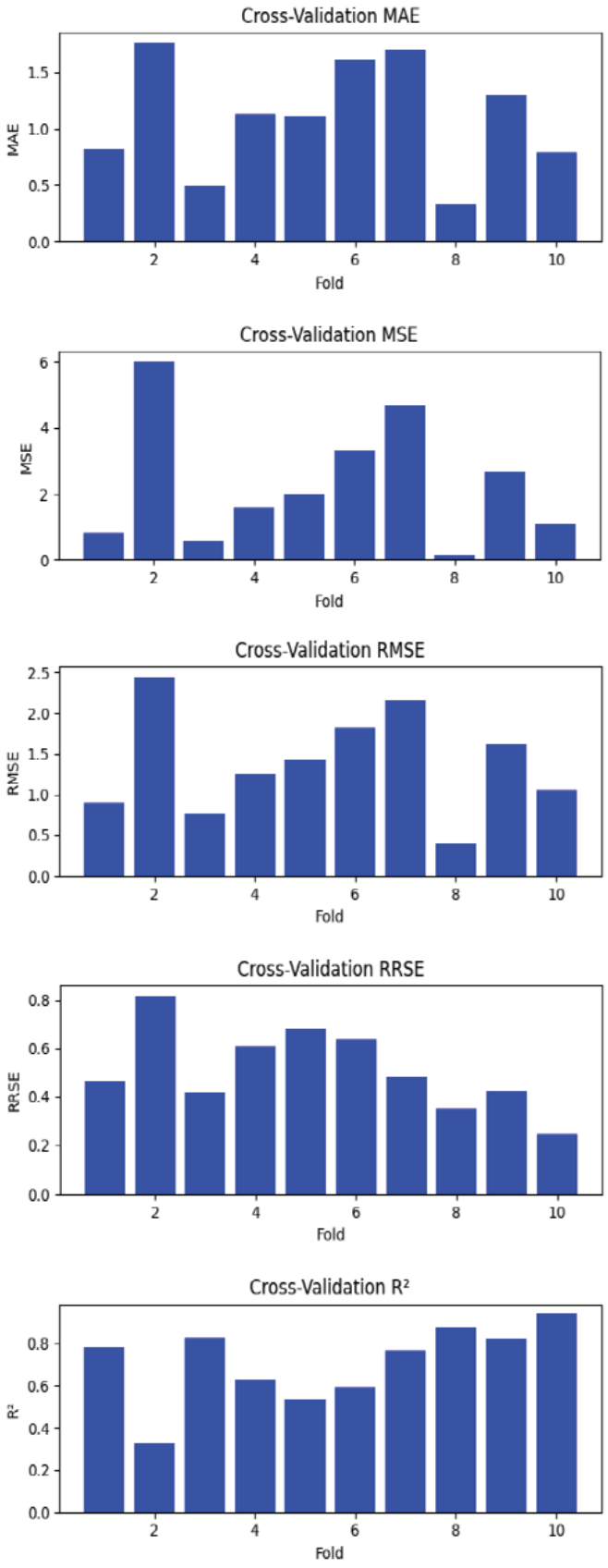

Fig. 9 28 day Flexural Strength K-fold cross validation for MAE, MSE, RMSE, RRSE and R-square
9. ábra A 28 napos hajlítószilárdság K-szörös keresztvalidációja MAE, MSE, RMSE, RRSE és R-négyzet értékekre

3.3.5 Sensitivity analysis

Predicting 28-days compressive strength showed iron stone maintaining dominance, with the water-cement ratio also playing a significant role as shown in *Fig. 10*. Regarding 28-days flexural strength prediction, iron stone was the primary influencer, followed by crushed granite and the water-cement ratio as shown in *Fig. 11*. Overall, iron stone consistently demonstrated the greatest influence across all assessed strengths, highlighting its crucial role in determining concrete's mechanical properties. The water-cement ratio consistently ranked among the top contributors, underscoring its significant impact on concrete performance. This analysis offers valuable insights for optimizing concrete mix designs and improving structural performance.

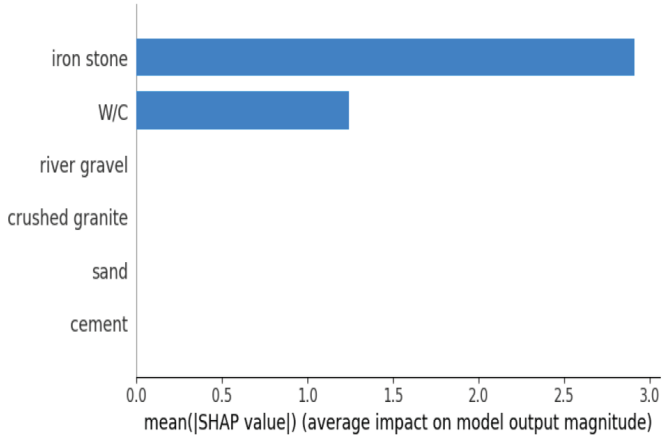

Fig. 10 28 day Compressive Strength Shapley average impact value
10. ábra A 28 napos nyomószilárdság Shapley-átlagos hatás értéke

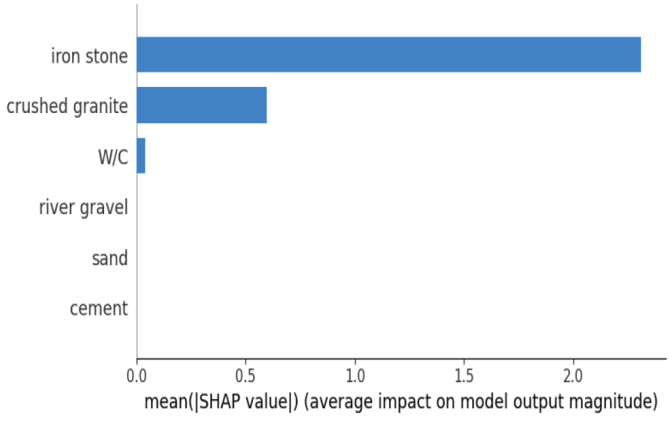

Fig. 11 28 day Flexural Strength Shapley average impact value
11. ábra A 28 napos hajlítószilárdság Shapley-átlagos hatás értéke

4. Conclusions

In this study, we applied a supervised machine learning approach to predict the compressive strength of concrete containing sedimentary aggregates. Gene Expression Programming (GEP) was employed for forecasting the compressive strength, demonstrating exceptional effectiveness through a high linear correlation coefficient (R^2) and minimal error values:

1. The GEP model effectively predicted compressive strengths at 7, 14, and 28 days with R-squared values exceeding 0.7 for both training and testing phases, indicating high precision and minimal errors. However, lower R-squared values for validation and higher error metrics suggest the need for model refinement to enhance generalization and performance on unseen data.
2. The model's reliability was confirmed through k-fold cross-validation for predicting compressive and flexural strengths, affirming its potential for practical applications in concrete strength prediction.
3. Iron stone significantly influenced all assessed strengths, highlighting its critical role in concrete's mechanical properties. The water-cement ratio and crushed granite also emerged as important factors, impacting compressive and flexural strengths. These insights are crucial for optimizing concrete mix designs and improving structural performance.
4. Ironstone shows potential for use as a coarse aggregate in concrete production, provided its physical characteristics such as high water absorption capacity, moisture content porosity, void ratio, poor grading, bulk density and specific gravity is adequately managed.

The application of GEP for predicting the compressive strength of concrete with sedimentary aggregates has proven effective and reliable, providing a foundation for further refinement and broader application of machine learning models in construction materials engineering.

Acknowledgement

The first author of this paper expresses a sense of gratitude to his post graduate supervisors, Michael Ebie Onyia and Godwin Oluwatosin Oyesanya for their immense contribution to the execution of the machine learning algorithm applied and also for their unquantifiable assistance in the execution and timely completion of the experimental programme.

Reference

[1] Ahmed, T., & Johnson, R. (2021). The role of ironstone aggregates in enhancing concrete strength. *Journal of Construction Materials*. 42(2): 158-170.

[2] Chen, Y., & Yang, F. (2019). Weathering resistance of ironstone and its application in concrete production. *International Journal of Civil Engineering*. 17(4): 422-430.

[3] Wu, L., Chen, Z., & Luo, Y. (2022). Admixtures in ironstone concrete: Balancing workability and strength. *Journal of Concrete Research*. 18(6): 279-287.

[4] Smith, R., White, B., & Williams, H. (2020). Mechanical properties of concrete with ironstone aggregates. *Materials Science Journal*. 55(4): 322-329.

[5] Li, X., & Zhao, J. (2021). Ironstone aggregates in marine concrete structures: A durability study. *Journal of Marine Structures*. 22(5): 197-210.

[6] Fatoye, F. B., Gideon, Y. B., & James, C. P. (2013). Geology and mineral resources of the Lower Benue Trough, Nigeria. *Pelagia Research Library. 4*(6): 21-28.

[7] El-Naggar, H., & Hassan, M. (2023). Sustainable construction: Utilizing ironstone in concrete production. *Sustainable Construction Journal*. 8(1): 12-25.

[8] Jain, P., & Patel, K. (2021). Enhancing concrete's mechanical properties using ironstone fines. *Construction Materials Journal*. 46(3): 230-245.

[9] Kumar, S., & Gupta, L. (2019). Analysis of ironstone's impact on concrete's weight and workability. *Civil Engineering Journal*. 14(2): 85-91.

[10] Hossain, M. D., Sadiq, R., & Shaw, D. (2017). Prediction of concrete compressive strength using gene expression programming. *Materials Science and Engineering. 228*: 012023. https://doi.org/10.1088/1757-899X/228/1/012023.

[11] Tayfur, G., & Yilmaz, M. (2019). Concrete mix design optimization using gene expression programming. *Engineering Applications of Artificial Intelligence. 78*: 264-276. https://doi.org/10.1016/j.engappai.2018.11.017.

[12] Zhang, L., Peng, Y., & Zhao, M. (2023). Machine learning approaches to optimize concrete with ironstone aggregates. *Advanced Concrete Technology*. 25(3): 102-113.

[13] Nunez, I., Marani, A., & Nehdi, M. L. (2020). Mixture optimization of recycled aggregate concrete using hybrid machine learning model. *Materials. 13*(19): 1-24. https://doi.org/10.3390/ma13194331.

[14] Mai, H. V. T., Nguyen, M. H., & Ly, H. B. (2023). Development of machine learning methods to predict the compressive strength of fiber-reinforced self-compacting concrete and sensitivity analysis. *Construction and Building Materials. 367*: Article 130339. https://doi.org/10.1016/j.conbuildmat.2023.130339.

[15] Inqiad, W. B., Raza, M. A., & Asim, M. (2023). Predicting 29-day compressive strength of self- compacting concrete (SCC) using gene expression programming (GEP). *Archive of Advanced Engineering Science. XX*(XX): 1-13. https://doi.org/10.47852/bonviewAAES32021606.

[16] Crina, M. O., & Groşan, G. (2003). A comparison of several linear genetic programming techniques. Retrieved from http://www.mep.cs.ubbcluj.ro.

[17] Alavi, A. H., Gandomi, A. H., Sahab, M. G., & Gandomi, M. (2010). Multi expression programming: A new approach to formulation of soil classification. *Engineering with Computers. 26*(2): 111-118. https://doi.org/10.1007/s00366-009-0140-7.

[18] Iftikhar, B., Alih, S. C., Vafaei, M., Elkotb, M. A., Shutaywi, M., Javed, M. F., Deebani, W., Khan, M. I., & Aslam, F. (2022). Predictive modeling of compressive strength of sustainable rice husk ash concrete: Ensemble learner optimization and comparison. *Journal of Cleaner Production, 348*, Article 131285. https://doi.org/10.1016/j.jclepro.2022.131285.

[19] Momoh, E. O., Atoo, A. A., & Nwakonobi, D. (2018). Suitability of Awka-North sedimentary stone as coarse aggregate for building construction. *International Journal of Engineering Science Inventio., 7*(1): 71-83.

[20] Farooq, F., Czarnecki, S., Niewiadomski, P., Aslam, F., Alabduljabbar, H., Ostrowski, K. A., Śliwa-Wieczorek, K., Nowobilski, T., & Malazdrewicz, S. (2021). A comparative study for the prediction of the compressive strength of self-compacting concrete modified with fly ash. *Materials. 14*(17): https://doi.org/10.3390/ma14174934.

[21] British Standards Institution. (2009). Testing hardened concrete. Compressive strength of test. (BS EN 12390-3:2009). London, UK: BSI.

[22] British Standards Institution. (1983). Testing concrete. Method for determination of flexural strength. (BS 1881-118:1983). London, UK: BSI.

[23] British Standards Institution. (1975/1988). Concrete. Complementary British standard to BS EN 206-1. (BS 8500-1 & BS 8500-2). London, UK: BSI.

Ref.:
Nwakonobi, Ugochukwu David – **Onyia**, M. E. – **Oyesanya**, O. G.: *Predicting 28-day compressive and flexural strengths of ironstone concrete using Gene Expression Programming (GEP)*
Építőanyag – Journal of Silicate Based and Composite Materials, Vol. 77, No. 2 (2025), 39–47 p.
https://doi.org/10.14382/epitoanyag-jsbcm.2025.6

Enhancement effect of polypropylene fiber on the characteristic properties of alkali-activated metakaolin-slag mortar

Huda M. ALNAJJAR ▪ Housing and Building National Research Centre, Cairo
H. M. KHATER ▪ Housing and Building National Research Centre, Cairo
Érkezett: 2025. 05. 13. ▪ Received: 13. 05. 2025. ▪ https://doi.org/10.14382/epitoanyag-jsbcm.2025.7

Abstract
Production of eco-friendly concrete is a global aim, to tackle this matter; Geopolymers have been identified as viable alternative replacements for ordinary Portland cement due to its excellent engineering properties and low CO_2 emissions. The advancement of geopolymer concrete (GPC) represents a significant milestone to make it more applicable and popular. An effort was made to investigate the impact of the blended Metakaolin (MK) and Ground Granulated Blast Furnace Slag (GGBFS) with Polypropylene Fiber (PPF) in various contents (0%, 0.5%, 0.1%, 1.5%, 2%, 2.5%) as reinforcement additive. For this, an experimental study was carried out to evaluate the effect of PPF on properties of the product. SEM, XRD, and FTIR analyses have been performed to determine the surface morphology and phases. Results show that incorporating PPF effectively reduces the shrinkage and improves its compressive strength compared with the control geopolymer mortar; optimum value was obtained with a PPF ratio of 0.5%.
Keywords: geopolymer, polypropylene fiber, metakaolin, slag, compressive strength.
Kulcsszavak: geopolimer, polipropilén szál, metakaolin, salak, nyomószilárdság

Huda Mohamed Abdelhaleem ALNAJJAR received her PhD degree in 2023, with a thesis focused on the synthesis, characterization, and development of sustainable polymeric composites and their applications, following an MSc in 2019 on nanomaterials for paint production. She is currently a researcher at the Housing and Building National Research Center (HBRC) in Egypt, where she has been working since 2017 in the raw materials department. She specializes in nanotechnology, sustainable materials, and instrumental analysis, with additional qualifications including a diploma in clinical biochemistry from Benha University (2020) and extensive training in analytical techniques such as TGA, DMA, and XRF.

Hisham Mustafa Mohamed KHATER received his PhD degree in Physical Chemistry in 2009 from Ain-Shams University, and is currently a Professor of Cement Chemistry and Raw Building Materials Technology at the Housing and Building National Research Center (HBRC) in Egypt, where he also supervises the accredited XRF laboratory. He specializes in geopolymer materials, waste recycling for sustainable building applications, and has authored or co-authored over 50 scientific publications in high-impact journals. He is a member of the Green Chemistry Network, American Chemical Society, Royal Society of Chemistry, and Society of Chemical Industry.

1. Introduction

The International Energy Authority (IEA) estimates that between 6 and 7 percent of all CO_2 emissions come from the production of Portland cement. In addition, the steel and aluminum industries consume the most energy, followed by the cement industry. In order to find solutions to these issues, numerous experiments have been carried out in order to identify new methods that can fulfill the requirements of the construction industry for an alternative to concrete [1]. 'Geopolymer' technology, coined by Davidovits, refers to the process of forming cement through the utilization of alkali minerals and aluminosilicates, Geopolymers are able to cure and harden at ambient temperatures [2]. When compared geopolymer to OPC, one of the most significant differences in the production process is that the production of OPC involves a high-energy manufacturing process "calcination". In contrast, Geopolymer employs industrial wastes (such as slags, fly ashes,...) which considered low-energy materials and a small quantity of high-energy materials (alkali hydroxides) to initiate a reaction. contrary to the hydration of Portland cement, just a limited quantity of H_2O has been used in the manufacturing of geopolymer gel; as a result, less mixing water is needed [3]. Finally, even though geopolymers exhibit less shrinkage than Portland cement materials, it is still an important consideration [4-6]. The incorporation of polypropylene fiber aims to create a geopolymer that is both strong and lightweight with low drying shrinkage. Polypropylene (PP) fibers are a set of synthetic fibers with certain features that arranged on a plastic matrix make them an excellent supplement to building materials *Fig. 1*. It is anticipated that the final geopolymer product will be appropriate for use as thermal insulation or fire resistance [7].

Noushini [8] employed the incorporation of polypropylene and polyolefin fibers to enhance the deformation and contraction characteristics of fly ash-based geopolymer with low calcium content. The findings indicated a reduction in drying shrinkage and an enhancement in compression creep within the geopolymer concrete, observed at both early and long-term stages, when a fiber volume fraction of 0.5% was added. Zhang et al. [9] investigated. The impact of polypropylene fiber on mechanical properties and volumetric stability, demonstrating that PP fiber can effectively bridge detrimental pores and defects. This modification alters the propagation pathways of cracks, leading to significant enhancements in both strength and toughness. Talib et al. [10] studied GPC preparation with (16M) of sodium hydroxide(NaOH), and with polypropylene fiber (PPF) and found there is a 50%, 30%, 16% enhancement in the flexural tensile strength, compressive strength, and split tensile strength with PPF addition. Haci Baykara et al. [11] Examined the interaction of PPF and zeolite-based geopolymer mortar and the influence of calcium hydroxide on the mechanical characteristics and thermal stability of the mortars and demonstrated that the optimum compressive strength was with PPF 0.5 wt.%. Zainab A. Mohammed et al. [12] revealed that The integration of PPF enhanced both the splitting tensile strength and the compressive strength.

Due to its high toughness and anticorrosion, (PPF) has been mostly used in reinforced cement and concrete industries. Although it was a conflict that stated that the incorporation of polypropylene fibers (PPF) significantly diminishes the compressive strength of concrete, Richardson [13] studied this conflict. He was noticed that the breaking of the cement bond due to the presence of PPF leads to a notable reduction in

the compressive strength of the concrete. Although the similar strength reduction was expected in geopolymer by PPF inclusion. Zhang et al. [9] stated that the initial compressive strength of the fly ash/calcined kaolin geopolymer exhibited an increase of approximately 68% and 20% at 1 and 3 days, respectively, by the incorporation of PPF in 0.5 wt%. Additionally, the early flexural strength of the composite with 0.75% PPF was doubled for both days. Navid Ranjbar et al. [7] evaluated that the addition of PPF up to 3 wt% to the geopolymer paste enhances the composites energy absorption and minimizes the shrinkage. However, depending on the fiber content, it may lower the material flexural and compressive strength.

Fig. 1 Polypropylene fiber used in this study
1. ábra A vizsgálatban használt polipropilén szál

Arash Karimipour and Jorge de Brito [14] evaluated the impact of silica fume (SF) and polypropylene fibers (PPF) on the mechanical behavior and fracture mechanics of ultra-high performance geopolymer concrete (UHPGC). The results of the experiments indicated that PPF is crucial in enhancing both mechanical and fracture characteristics of UHPGC that contains SF and PPF.

Aisheh, Y. et al. [15] studied the presence of hybrid fibers in a GPC which successfully aids in the transition to a softer state and successfully reduces abrupt failure. According to Sangi, R. et al. [16] adding 1% steel fibers and 0.1% PPF in a Geopolymer Concrete specimen, significantly increases displacement ductility factor and capacity of energy absorption. Also Sangi, R. et al. [17] emphasized that the type and dosage of fiber affect the mechanical properties of GPC; the compressive strength was used to determine the ideal fiber dosage for different grades of GPC. By varying the fiber percentage, they found that the optimal dosage for polypropylene fibers in geopolymer concrete was 0.6%.

The objective of this paper is to examine the impact of the incorporation of polypropylene fibers to geopolymer matrix through measuring XRD, FTIR, mechanical properties, drying shrinkage and also their thermal stability compared to control mix. The goal is to identify the most effective matrix which can be applied in construction applications.

2. Materials and methods

Geopolymers or Alkali-activated materials (AAMs) are a class of inorganic binders that are formed by reacting aluminosilicate materials with an alkaline solution

2.1 Raw materials

The materials used in this study are Metakaolin (MK) obtained from Aluminum Sulfate Co. of Egypt (ASCE) and Ground Granulated Blast Furnace Slag (GGBS) obtained from Iron and Steel factory, Helwan, Egypt as starting materials. Polypropylene fiber 12 mm length obtained from polyfibers company (Turkey) used as additive in ratios 0.5, 1, 1.5, 2, 2.5%. *Table 1* shows the chemical composition of MK and GGBFS used in this work. *Fig. 2* shows the XRD patterns of MK and GGBS. Liquid Sodium Silicate LSS (Na_2SiO_3) used in the present work received from Fisher company and has a density of 1.46 g/cm^3, it was mixed proportionally at equal volume of (NaOH) solution as alkali activator. In order to prevent coagulation of the added fiber, superplasticizer was obtained from Sika Company and added in various ratios from the total weight of binder for better dispersion of the added compositions.

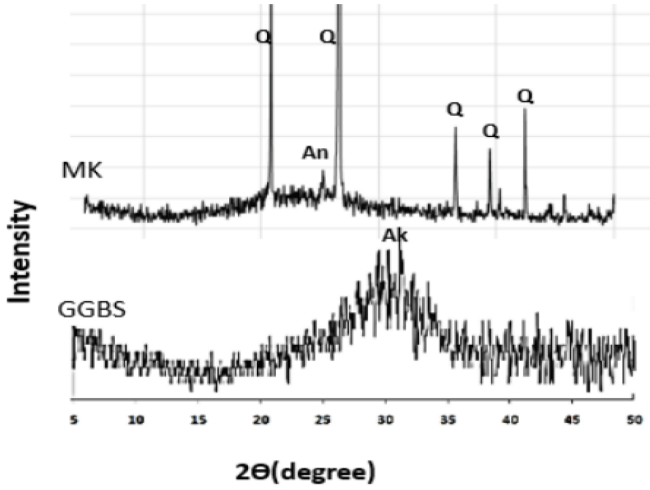

Fig. 2 XRD pattern of starting raw materials (Q= Quartz, An= Anataze, AK= Akermanite)
2. ábra A kiindulási nyersanyagok röntgendiffrakciós (XRD) mintázata (Q = kvarc, An = anatáz, AK = akermanit)

Materials	SiO_2	Al_2O_3	Fe_2O_3	CaO	MgO	Na_2O	K_2O	SO_3	TiO_2	L.O.I	Total
MK	61.1	31.4	1.51	0.32	0.11	0.12	0.14	0.13	2.44	2.33	99.6
GGBFS	36.59	10.1	1.84	33.07	6.43	1.39	0.74	3.52	0.52	–	99.96

Table 1 Chemical composition of MK and Slag
Table 1 Chemical composition of MK and Slag

2.2 Methods

Geopolymer mortar activated by using an equal volume of sodium hydroxide (NaOH, 7M) and liquid sodium silicate LSS (Na_2SiO_3). PPF was added at ratios of 0.5, 1, 1.5, 2, and 2.5% by powder mass. Sonication used for well dispersion. Mixes were poured into 2.5 cm length cubic molds, smoothed with a thin edged trowel, and cured at room temperature for 24 hours, the demolded specimens cured at 40 °C with 100% relative humidity. Specimens were taken out from their curing condition, dried at 80 °C for 24 hours, then tested for compressive strength. To prevent further hydration, the crushed specimens being dried at 105 °C until the testing time, it kept in an airtight container. Compressive strength was carried out at 7, 21, 28, 60 and 90 days according to ASTM C109 M [18]. All the prepared mixes of different materials were left to be cured at the lab ambient condition of 25 °C for 24 hrs. Then, subjected to curing temperature of 40°C at a 95±5% relative humidity in a controlled humidity chamber. *Table 2* shows the geopolymer mix design for the mortar.

mixes	GGBFS%	MK%	PPF%	SH (7M)	LSS	SP	w/b
SMP0	50	50	0	0.125	0.125	0.8	0.250
SMP1	50	50	0.5	0.125	0.125	1.0	0.250
SMP2	50	50	1	0.125	0.125	1.2	0.250
SMP3	50	50	1.5	0.130	0.130	1.4	0.260
SMP4	50	50	2	0.130	0.130	1.6	0.260
SMP5	50	50	2.5	0.130	0.130	1.8	0.260

Table 2 The composition and designation of the different mixes.
2. táblázat A különböző keverékek összetétele és jelölése

2.3 Investigation Methods

Starting materials investigated by using XRF-Axios (PW4400) WD-XRF Sequential Spectrometer Netherland, while mineralogical characterization was done by Philips PW 3050/60 diffractometer using a Cu-Kα source. The infrared spectral analysis used for elucidation of the amorphous constituents of geopolymer composites using Jasco-6100 –America, with the aid of KBr binder in the range from 400 to 4000 cm^{-1}. Mechanical testing was performed using 5 tons German Brüf digital compression testing machine with a loading rate of 100 kg/min [19, 20]. Morphology of the hydration products was examined by scanning electron microscope (SEM) Inspect S (FEI Company, Netherlands) equipped with an energy-dispersive X-ray analyzer (EDX). Drying shrinkage percent was calculated at ages of 28 and 90 days of curing. The thermo-mechanical properties tested for the composites by exposing them to high temperatures in the furnace. After curing at 28 d each sample subjected to thermal treatment at 300 °C, 500 °C and 800 °C at a sustained period of 2 h. weight loss, firing shrinkage and residual percent of the strength were calculated.

3. Results and discussion

Experimental studies were established to examine the impact of PPF on geopolymer mortars and Determine the best added ratio.

3.1 Fourier Transform Infrared Spectroscopy FTIR

Fig. 3 represents the FTIR spectra of alkali-aktivated mortar having various ratios of PPF. A significant peak is observed within the wavenumber range of 3467-3434 cm^{-1}, which is associated with the stretching vibration of the O–H bond found in hydroxyl groups present in water molecules or CSH and CASH phases. The presence of hygroscopic water is evidenced by the peaks detected in the range of 1645-1638 cm^{-1}, attributed to the bending vibrations of water molecules within the amorphous matrix of the geopolymer mortars [21]. The observed peaks in the range of approximately 3000–2800 cm^{-1} can be attributed to the presence of CH2 groups, which mainly from the inclusion of polypropylene within the geopolymer matrix. The increased broadness of O-H vibration band at 3467-3434 cm^{-1} favors the increased formation of CSH and CASH with polypropylene up to 0.5%. This is coherent with the increased intensity of asymmetric T-O-Si of amorphous geopolymer and decreased the intensity of non soulibilized silica at about 1100 cm^{-1} which dissolved by the enhancement effect of activator as well as the addition of polypropylene. The observed peak within the wavenumber range of 1455 to 1426 cm^{-1} can be attributed to the stretching vibration of the O–C–O bond, resulting from the formation of calcium carbonate and sodium carbonates. [7, 22].

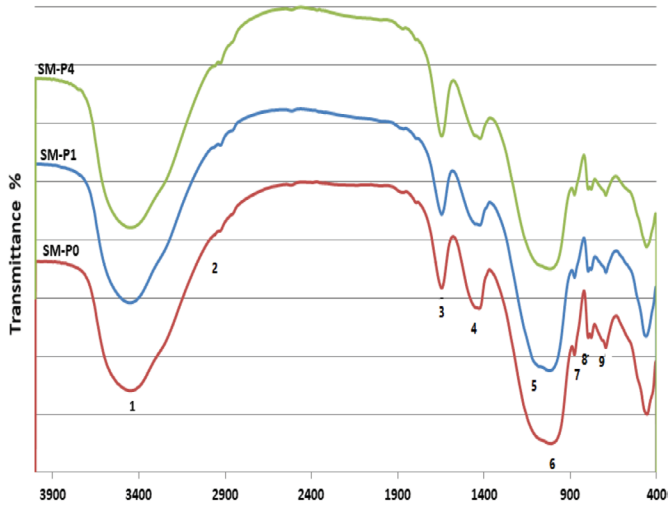

Fig. 3 FTIR spectra of 90 days alkali-activated composite having various ratios of PPF.
(1: OH asymmetric and symmetric stretching vibration, 2: bending vibration of (HOH), 3: stretching vibration of CO_2, 4: asymmetric stretching vibration (Si–O–Si), 5: asymmetric stretching vibration (T–O–Si), 6: symmetric stretching vibration of CO2,7: symmetric stretching vibration (A1–O–Si), 8: symmetric stretching vibration (Si–O–Si), 9: bending vibration (Si–O–Si and O–Si–O))
3. ábra A 90 napos lúgosan aktivált kompozit FTIR spektrumai különböző PPF arányok mellett.
(1: OH aszimmetrikus és szimmetrikus nyúlási rezgés, 2: (HOH) hajlítási rezgés, 3: CO_2 nyúlási rezgés,4: (Si–O–Si) aszimmetrikus nyúlási rezgés, 5: (T–O–Si) aszimmetrikus nyúlási rezgés, 6: CO_2 szimmetrikus nyúlási rezgés, 7: (Al–O–Si) szimmetrikus nyúlási rezgés, 8: (Si–O–Si) szimmetrikus nyúlási rezgés, 9: (Si–O–Si és O–Si–O) hajlítási rezgés)

3.2 XRD Analysis

Fig. 4 shows the X-ray diffraction patterns of 90 days GGBFS –MK composites without and with PPF for specimens dosages 0.5% and 2%, It was consisted mainly from quartz as crystalline phases, a rise between hump in the region 20 and 35° in 2θ, which is a normal behavior in amorphous materials related to geopolymer matrix, observed for specimens with dosage of 0.5% PPF. When dosage increased the degree of crystallinity increase. Forming intense peak of sodalite which is one of the zeolites, in addition to the increased intensity of calcite as a result of carbonation of unreacted sodium ions [11]. The figure reflects also the absence of calcite peak at 23.05° where most of the added alkalis consumed in the geopolymer formation and not subjected to carbonation. This will lead to an increased porosity within the matrix. XRD analysis demonstrated that the addition of PPF to the geopolymer matrix did not lead to the emergence of any new crystalline phases within the composite material.

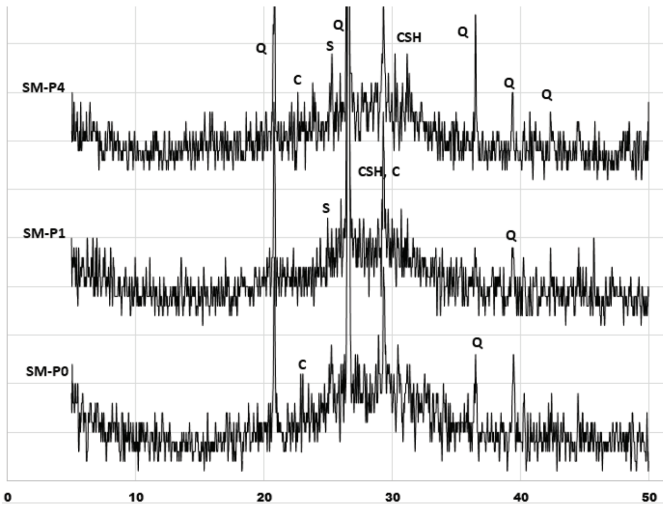

Fig. 4 X-ray diffraction pattern of 90-days alkali activated GGBFS-MK composite with various ratios of PPF (Q: Quartz, C: Calcite, S: Sodalite, CSH: Calcium Silicate Hydrate)

4. ábra A 90 napos lúgosan aktivált GGBFS–MK kompozit röntgendiffrakciós mintázata különböző PPF arányok mellett (Q: kvarc, C: kalcit, S: szodalit, CSH: kalcium-szilikát-hidrát)

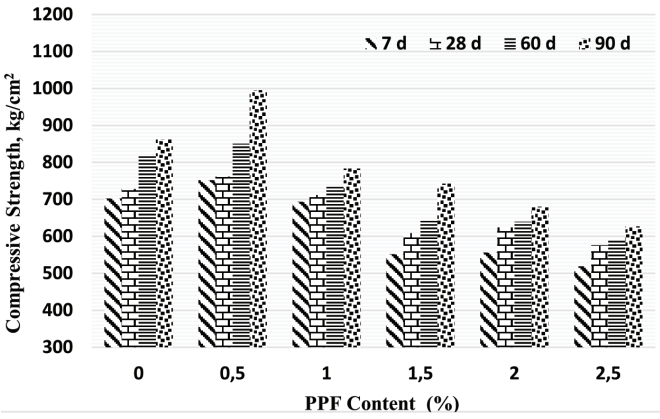

Fig. 5 Compressive strength of GGBFS-MK matrix with various ratios of PPF

5. ábra A GGBFS–MK mátrix nyomószilárdsága különböző PPF arányok mellett

3.3 Compressive Strength

The utilization of PPF as a reinforcing agent within alkali activated matrix presents significant advantages, suggesting that these plastics / polymers may be suitable for recycling and warrant evaluation for their potential applications in the construction and civil engineering sectors [7]. The composite material reinforced with 0.5 wt.% PPF exhibits a significant enhancement in compressive strength relative to the other samples. Conversely, the mechanical performance of the composites containing the highest concentration of polypropylene fibers was negatively impacted (>0.5 wt.%). This negative effect is most likely caused by the PPF heterogeneous distribution and agglomeration within the geopolymer mortar matrix. The less workability of geopolymer mortars would lead to the decrease in collision of the reactants which cause the formation of geopolymer. *Fig. 5* indicates that an increase in the percentage of PPF correlates with a decrease in mechanical resistance. This observation aligns with the reduced workability exhibited by the mixtures, which can be attributed to the minimal interaction between the nonpolar characteristics of PPF and the polar nature of the geopolymeric matrix.

3.4 Scanning Electron Microscopy

Fig. 6 shows Scanning Electron Microscopy pictures of the geopolymer both with and without PPF and revealing a notable presence of amorphous material. *Fig. 6/B* showed more compact matrix by the coupling of polypropylene fiber (0.5%) with geopolymer matrix compared with control mix (0.0%) *Fig. 6/A*. The dense and amorphous matrix is mainly associated with the geopolymeric structure (calcium silicate hydrate) that develops during the preparation of the geopolymer. By increasing polypropylene fiber content (2%) it seems that PPF did not undergo any chemical degradation and it didn't have a chemical bond with the aluminosilicate matrix *Fig. 6/C*. These results supported by similar studies [23, 24] which suggested that the morphology of PPF explained the low mechanical properties of geopolymers reinforced with. The observed low compressive strength in reinforced composites with a high content of PPF can be attributed to the influence of hydrophobicity and the contraction that takes place during the fiber-matrix interaction.

3.5 Drying Shrinkage

Numerous research investigations have demonstrated that the interaction of fiber content plays a crucial role in regulating the shrinkage of reinforced geopolymer composites [24]. *Fig. 7* shows the influence of PPF on controlling the shrinkage of GGBFS-MK geopolymer. PPF can bridge cracks and stop them from growing, and its incorporation, even in small amounts (0.5%), can greatly reduce the drying shrinkage of the composite specimens [25]. While, an adverse effect with the increase in fiber content to 2.5%. This can be attributed to the poor compactness of the geopolymer composition and these types of plastics polymers. Finally, the addition of PPF to geopolymer improves the uniformity of matrix and reduces the porosity.

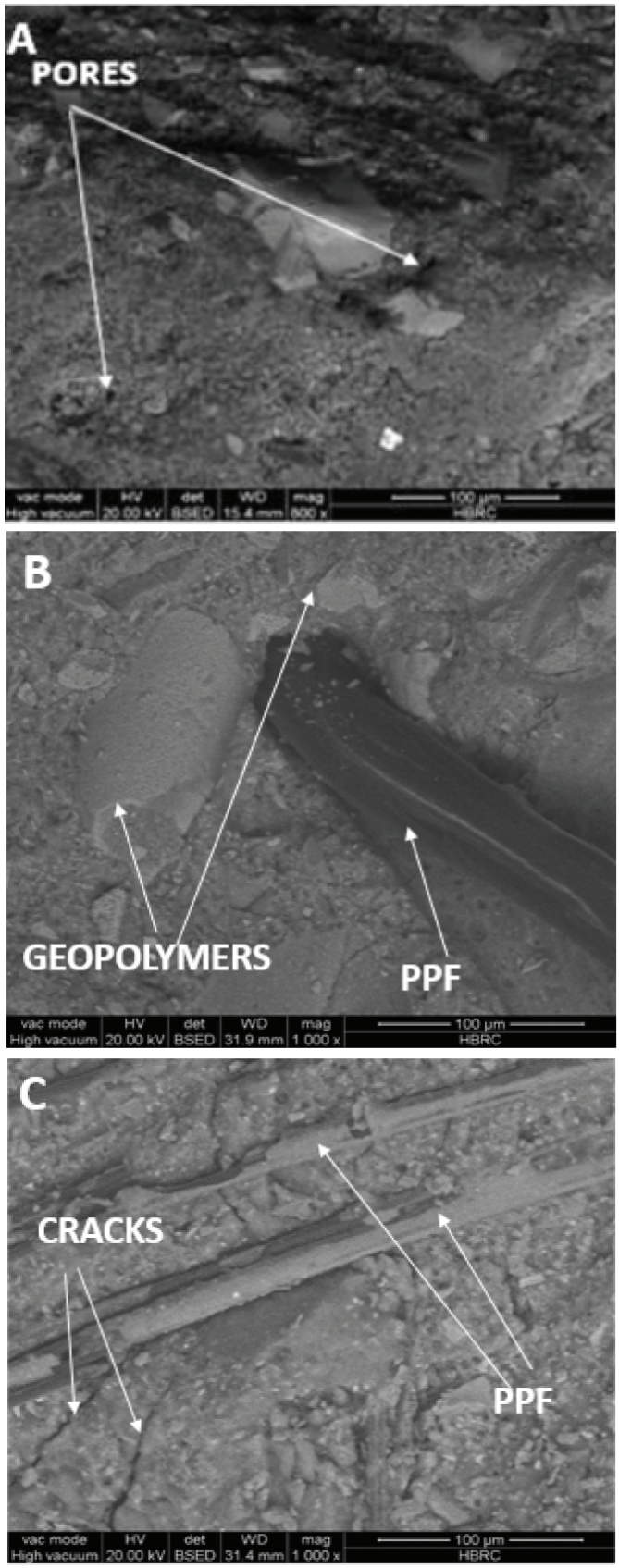

Fig. 6 SEM of 90 days alkali- activated GGBFS-MK geopolymer containing PPF in varies ratios
A: 0%, B: 0.5% and C: 2%
6. ábra A 90 napos lúgosan aktivált GGBFS–MK geopolimer SEM-felvétele különböző PPF arányokkal
A: 0%, B: 0,5%, C: 2%

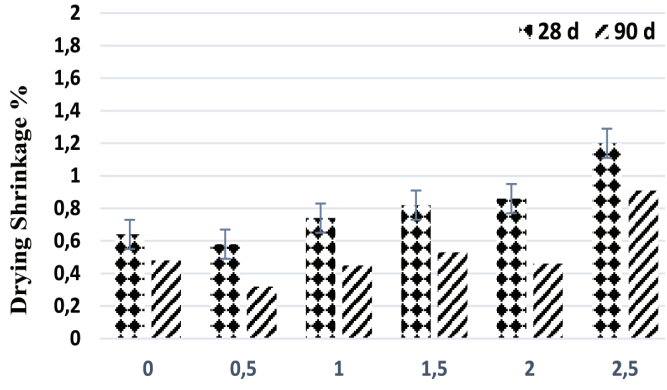

Fig. 7 Drying Shrinkage of all mixes at 28 and 90 days of curing
7. ábra Az összes keverék száradási zsugorodása 28 és 90 napos érlelés után

3.6 Thermal resistance

In this section, we are going to study the effect of firing on neat GGBFS-MK and GGBFS-MK coupled with 0.5% PPF (the optimum ratio). At 300, 500 and 800 °C for 2 hours with heating rate 5 °C/min. There are various parameters that will be monitored in this section: mass loss, firing shrinkage and residual compressive strength via strength change factor (SCF).

3.6.1 Mass loss

Generally, the increase in temperature of firing leads to an increase in mass loss percentage as known for all geopolymer matrices. Evaporation of free water and some chemically bonded water from geopolymers results in mass loss between room temperature and 300 °C, t might be linked to the hydration products degradation Al-OH, Si-OH, and Ca-OH groups dehydroxylate at 300–550 °C. More than 750 °C the mass loss is related to the carbonate species decomposition [26, 27]. The mass loss for control specimen was 5.05, 7.5 and 8.8% at 300, 500 and 800 °C respectively. *Fig. 8* shows that the mass loss of PPF paste was lower than that of control mix. At about 170 °C, PP fibers melt and create more voids, which help reduced the built-up internal vapor pressure. At 300 °C, the first weight loss occurs [28]. On the other hand, since the melting of higher amount of PPF led to higher amount of mass loss for the exposed temperatures of 500 and 800 °C, the weight loss for all pastes was nearly the same. Giving 4.45, 7.2 and 8.3% by mass loss reduction 12, 4, and 6% at 300, 500 and 800°C respectively.

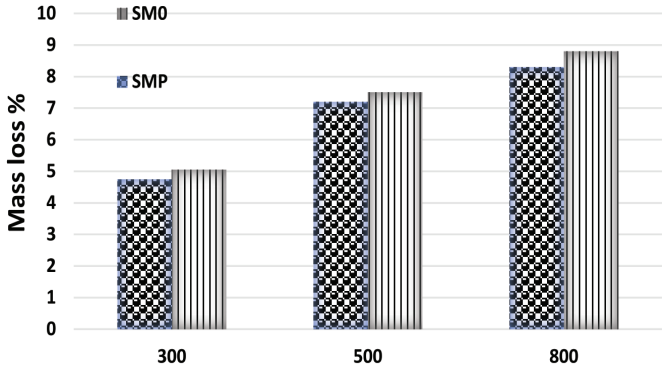

Fig. 8 Weight loss% for mixes versus treatment temperatures
8. ábra Tömegveszteség (%) a keverékek esetében a kezelési hőmérsékletek függvényében

3.6.2 Firing shrinkage

Behaviour of Cracking and smashing up the geopolymer could be noticed on account of contracted pores, free water evaporated from the pores leading to cracks propagation resulting in shrinkage correspondingly. The appearance of a considerable shrinkage leading to cracks. In the temperature range of 100 °C–300 °C, early shrinkage occurs because of dewatering. Up to 500 °C, the growth occurred continually, at a temperature of 800 °C, a notable size reduction was observed. The thermal shrinkage of geopolymers at 28 days of age exhibited an increase in response to rising temperatures, as illustrated in the accompanying *Fig. 9*. Average of firing shrinkage % can be calculated using the formula below:

$$F.S\ \% = (DL-FL)/DL^{*}100$$

Where: DL for dried length and FL for fired length.

The Figure shows that the treated specimen had a lower shrinkage value than the control one. The thermal shrinkage was brought on by the removal of free water during the poly-condensation stage. Additionally, capillary tensions were created as a result of this process, drawing the particles together and producing more water as the temperature rose [29]. The significant increase in thermal shrinkage that happened when the geopolymer was heated to 800 °C is probably due to the formation of a new crystalline phase. At temperature 300 °C and 500 °C there was a slightly shrinkage increased, but at 800°C, there was a significant shrinkage increase. Finally, geopolymer treated with polypropylene fiber gives firing shrinkage 1.5, 2.4 and 9.14% by shrinkage reduction 53, 37 and 24% at 300 °C, 500 °C and 800 °C respectively.

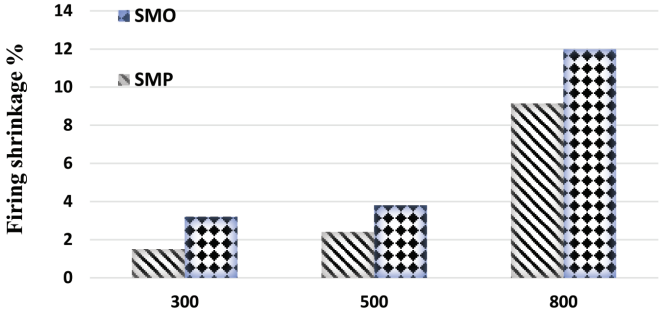

Fig. 9 Firing shrinkage of all mixes versus temperatures 300, 500 and 800°C
9. ábra Az összes keverék égetési zsugorodása 300, 500 és 800 °C hőmérsékleteken

3.6.3 Strength Change Factor (SCF)

Geopolymers formed from rich aluminosilicate materials offer an enhancement of the geopolymers strength at room temperature, but sometimes not when subjected to high temperatures. The strength of geopolymer paste depends on two contradictory processes, the damage process because of the thermal effect and the process of further geopolymarization. Transformation of amorphous geopolymer constituents into crystalline feldspars depending on the composition of the matrix. to calculate the average of Strength Change Factor, the equation below can be used.

$$SCF\ \% = (S_0-S_f)/S_0^{*}100$$

Where: S_0 = strength after drying at 80°C and S_f = strength after firing. The strength change factor versus temperature is represented in *Fig. 10*. Control geopolymer gives 5.5, 7.4 and 31% at 300 °C, 500 °C and 800 °C respectively. The compressive strength of geopolymer treated with PPF were -8.33% (strength gain), 4.08 and 6.05% after heating to 300° C, 500 °C and 800 °C respectively. Firing at 300 °C resulted in increased geopolymerization reaction of the system thus the compressive strength increased slightly. In addition, Ju et al. [30] explained by Van der Waals force that the evaporation of free water at 300 °C caused the gel layer in matrix to come closer together which also led to the increase in strength of matrix. At high temperature the compressive strength reduced which may be due to the decomposition of calcium resulting in the deterioration of alkali-activated paste.

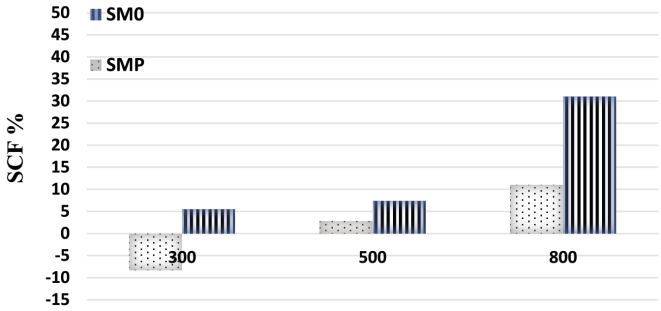

Fig. 10 Strength Change Factor (SCF) % for mixes versus temperature temperatures 300, 500 and 800°C.
10. ábra A szilárdságváltozási tényező (SCF) % a keverékek esetében 300, 500 és 800 °C hőmérsékleteken

4. Conclusions

This study courage using geopolymers for enhancing environmental safety and sustainability in construction through reduction of CO_2 emission and re-use of industrial by-products (waste management). Addition of PPF enhances the mechanical strength via bridging effect making it very appropriate to use in constructions that require high mechanical properties as bridges & dams.

Conclusion can be drawn according to the experimental results:

1. Addition of PPF enhanced the strength of geopolymer matrix the suitable content percent was 0.5% Where it recorded the highest compressive strength.
2. The addition of PPF reduced drying shrinkage of geopolymer matrix as compared with control mix.
3. Incorporation of PPF within the geopolymer paste enhanced thermal properties after firing of specimens at 300, 500 and 800 °C by measuring of mass loss, drying shrinkage and strength change factor

Conflicts of Interest

The authors declare no conflicts of interest.

References

[1] Herbert Sinduja, J., N. Sakthieswaran, and G. Shiny Brintha, *Review on geopolymer concerte with different additives.* Int. J. Eng. Res. IJOER, 2015. **1**: p. 21-31.

[2] Mackenzie, K. and M. Welter, *Geopolymer (aluminosilicate) composites: synthesis, properties and applications*, in *Advances in ceramic matrix composites*. 2014, Elsevier. p. 545-568.

[3] Perera, D., et al., *Influence of curing schedule on the integrity of geopolymers.* Journal of materials science, 2007. **42**: p. 3099-3106.

[4] Kuenzel, C., et al., *Ambient temperature drying shrinkage and cracking in metakaolin-based geopolymers.* Journal of the American Ceramic Society, 2012. **95**(10): p. 3270-3277.

[5] Zuhua, Z., et al., *Role of water in the synthesis of calcined kaolin-based geopolymer.* Applied clay science, 2009. **43**(2): p. 218-223.

[6] Ridtirud, C., P. Chindaprasirt, and K. Pimraksa, *Factors affecting the shrinkage of fly ash geopolymers.* International Journal of Minerals, Metallurgy, and Materials, 2011. **18**(1): p. 100-104.

[7] Ranjbar, N., et al., *A comprehensive study of the polypropylene fiber reinforced fly ash based geopolymer.* PloS one, 2016. **11**(1): p. e0147546.

[8] Noushini, A., A. Castel, and R.I. Gilbert, *Creep and shrinkage of synthetic fibre-reinforced geopolymer concrete.* Magazine of Concrete Research, 2019. **71**(20): p. 1070-1082.

[9] Zhang, Z.-h., et al., *Preparation and mechanical properties of polypropylene fiber reinforced calcined kaolin-fly ash based geopolymer.* Journal of Central South University of Technology, 2009. **16**(1): p. 49-52.

[10] Talib, A., et al., *Effects of Polypropylene Fibre on Strength of Geopolymer Concrete*. DOI.

[11] Baykara, H., et al., *Preparation, characterization, and evaluation of compressive strength of polypropylene fiber reinforced geopolymer mortars.* Heliyon, 2020. **6**(4).

[12] Mohammed, Z.A., L.A. Al-Jaberi, and A.N. Shubber, *Effect of polypropylene fiber on properties of geopolymer concrete based metakolin.* Journal of Engineering and Sustainable Development, 2021. **25**(2): p. 58-67.

[13] Richardson, A.E., *Compressive strength of concrete with polypropylene fibre additions.* Structural survey, 2006. **24**(2): p. 138-153.

[14] Karimipour, A. and J. de Brito, *RETRACTED: influence of polypropylene fibres and silica fume on the mechanical and fracture properties of ultra-high-performance geopolymer concrete*. 2021, Elsevier.

[15] Aisheh, Y.I.A., et al., *Influence of polypropylene and steel fibers on the mechanical properties of ultra-high-performance fiber-reinforced geopolymer concrete.* Case Studies in Construction Materials, 2022. **17**: p. e01234.

[16] Sangi, R., B. Srinivas, and K. Shanker, *Mechanical Properties of Geo Polymer Concrete (GPC) by Using Steel, Polypropylene and Glass Fibers.* Indian Journal of Science and Technology., 2023. **16**(41): p. 3648-3656.

[17] Sangi, R., S.S. Bollapragada, and S. Kandukuri, *Sciendo.* Slovak Journal of Civil Engineering, 2024. **32**(3): p. 13-20.

[18] Standard, A., *ASTM C109-standard test method for compressive strength of hydraulic cement mortars.* ASTM International, West Conshohocken, PA, 2008.

[19] de Vargas, A.S., et al., *Strength development of alkali-activated fly ash produced with combined NaOH and Ca (OH) 2 activators.* Cement and concrete composites, 2014. **53**: p. 341-349.

[20] Khater, H. and M. Ghareib, *Utilization of alkaline Aluminosilicate activation in heavy metals immobilization and producing dense hybrid composites.* Arabian Journal for Science and Engineering, 2021. **46**(7): p. 6333-6348.

[21] Alomayri, T., F. Shaikh, and I.M. Low, *Mechanical and thermal properties of ambient cured cotton fabric-reinforced fly ash-based geopolymer composites.* Ceramics International, 2014. **40**(9): p. 14019-14028.

[22] Nikolov, A., I. Rostovsky, and H. Nugteren, *Geopolymer materials based on natural zeolite.* Case Studies in Construction Materials, 2017. **6**: p. 198-205.

[23] Han, B., S. Ding, and X. Yu, *Intrinsic self-sensing concrete and structures: A review.* Measurement, 2015. **59**: p. 110-128.

[24] Gomis, J., et al., *Self-heating and deicing conductive cement. Experimental study and modeling.* Construction and Building Materials, 2015. **75**: p. 442-449.

[25] Rashad, A.M., *The effect of polypropylene, polyvinyl-alcohol, carbon and glass fibres on geopolymers properties.* Materials Science and Technology, 2019. **35**(2): p. 127-146.

[26] Resende, H.F., et al., *Residual mechanical properties and durability of high-strength concrete with polypropylene fibers in high temperatures.* Materials, 2022. **15**(13): p. 4711.

[27] Zhang, Y.J., S. Li, and Y.C. Wang, *Microstructural and strength evolutions of geopolymer composite reinforced by resin exposed to elevated temperature.* Journal of Non-Crystalline Solids, 2012. **358**(3): p. 620-624.

[28] Zhang, P., et al., *A review on properties of fresh and hardened geopolymer mortar.* Composites Part B: Engineering, 2018. **152**: p. 79-95.

[29] Castillo, C., *Effect of transient high temperature on high-strength concrete.* 1987: Rice University.

[30] Ju, Y., et al., *An experimental investigation of the thermal spalling of polypropylene-fibered reactive powder concrete exposed to elevated temperatures.* Science bulletin, 2015. **60**(23): p. 2022-2040.

Ref.:

Alnajjar, Huda M. – **Khater**, H. M.: *Enhancement effect of polypropylene fiber on the characteristic properties of alkali-activated metakaolin-slag mortar*

Építőanyag – Journal of Silicate Based and Composite Materials, Vol. 77, No. 2 (2025), 48–54 p.

https://doi.org/10.14382/epitoanyag-jsbcm.2025.7

Use of recycled glass fiber-epoxy resin as additive for mullite ceramics

Emese Kurovics ▪ Institute of Energy, Ceramics and Polymer Technology, University of Miskolc ▪ emese.mesterne@uni-miskolc.hu

Habtamu Mnichl ▪ Institute of Energy, Ceramics and Polymer Technology, University of Miskolc ▪ habteched@gmail.com

Monika Tokár ▪ Institute of Metallurgy, Metal Forming and Nanotechnology, University of Miskolc ▪ monika.tokar@uni-miskolc.hu

Érkezett: 2025. 06. 18. ▪ Received: 18. 06. 2025. ▪ https://doi.org/10.14382/epitoanyag-jsbcm.2025.8

Abstract

The use of recycled materials in ceramic production is becoming increasingly important in the development of more sustainable and cost-effective materials. This study focuses on the use of recycled glass fiber-reinforced epoxy resin (GFRE) powder, produced by mechanical grinding, as an additive in mullite-based ceramic systems. The goal is to investigate how the addition of this composite powder affects mullite formation and the physical properties of the fired ceramic specimens. The main aim of the study is to determine whether the recycled GFRE powder can act as a reactive filler that promotes mullite formation at lower temperatures, and whether it has any effect on the porosity or other characteristics of the sintered ceramics. X-ray diffraction (XRD) and scanning electron microscopy (SEM) will be used to analyze the phase composition and microstructure of the samples. Using GFRP waste as a ceramic additive offers a novel way to recycle difficult-to-process composite materials. This approach may contribute to the development of more sustainable ceramic technologies and provide a practical solution for reusing industrial composite waste in high-temperature applications.

Keywords: ceramics, glass fiber, GFRE, mullite, SEM, XRD
Kulcsszavak: kerámiák, üvegszál, GFRE, mullit, SEM, XRD

Emese KUROVICS
received her PhD degree in 2022 from the University of Miskolc, where she is currently working as a research fellow at the Institute of Energy, Ceramics and Polymer Technology. She is the author or co-author of more than 70 scientific articles and a member of the Scientific Society of the Silicate Industry.

Habtamu MNICHL
is currently participating in the AMIR Master's Double Degree Program at the University of Miskolc and the Universidad Politécnica de Madrid. His areas of specialization include materials engineering and the circular economy.

Monika TOKÁR
is currently working as an assistant lecturer at the Institute of Metallurgy, Metal Forming, and Nanotechnology at the University of Miskolc. She is the author or co-author of more than 60 scientific publications.

1. Introduction

Mullite ($3\ Al_2O_3 \cdot 2\ SiO_2$) is a highly desirable ceramic material due to its excellent thermal stability, low thermal conductivity, high refractoriness, and superior mechanical strength at elevated temperatures [1, 2]. These properties make it suitable for demanding applications in the fields of advanced refractories, thermal insulation, and structural ceramics [3]. However, the synthesis of mullite traditionally requires high-purity raw materials and elevated sintering temperatures (typically >1200 °C), which contribute to significant energy consumption and environmental impact [4, 5].

To address these concerns, growing research efforts have focused on incorporating industrial by-products and waste materials into mullite-based ceramics to reduce production costs and improve sustainability [6-10]. Kaolin, a naturally occurring aluminosilicate, and alumina are common starting materials, but recent studies have demonstrated the potential of using silica- or alumina-containing waste – such as fly ash, glass waste, or ceramic sludge – to aid mullite formation and modify the microstructure of the resulting ceramics [11-15]. Glass fiber-reinforced epoxy (GFRE) composite waste, originating from end-of-life composite products, represents a particularly challenging and underutilized material for recycling due to its thermoset nature and mixed inorganic-organic composition [16, 17].

In this context, this study investigates the use of recycled GFRE powder – produced by mechanical grinding of composite waste – as an additive in kaolin-alumina-based ceramic formulations. The primary objective is to evaluate whether the GFRE powder can function as a reactive filler that contributes to mullite formation at lower temperatures, possibly through the release of SiO_2 and fluxing agents during thermal decomposition [18, 19]. In addition, the influence of GFRE on the porosity, microstructure, and phase composition of the sintered ceramics is examined [20].

To characterize the effect of the GFRE addition, X-ray diffraction (XRD) is employed to identify and quantify the crystalline phases formed during firing, while scanning electron microscopy (SEM) provides insights into the morphology and distribution of mullite crystals and the porosity of the ceramic matrix [21-23]. These analyses aim to clarify the relationship between composite waste addition and microstructural evolution, thereby assessing the feasibility of using GFRE as a functional ceramic additive [24].

The integration of GFRE waste into ceramic systems offers a promising strategy for recycling composite materials that are otherwise difficult to process [25]. By valorizing this waste stream within high-temperature ceramic applications, the proposed approach contributes to the advancement of circular economy practices and the development of more sustainable ceramic technologies [26, 27].

2. Materials and methods

Ceramic mixtures were prepared using Nabalox 315 alumina and Sedlecky ml kaolin as alumina- and silica-based raw materials, respectively. The formulations were prepared both with and without the addition of recycled glass fiber-reinforced epoxy (GFRE) powder, as summarized in *Table 1*.

Mixture sign	Sedlecky ml kaolin	Nabalox 315 alumina	Glass fiber-reinforced epoxy resin as additive
I.	76.71	23.29	0
II.	76.71	23.29	2.5
III.	76.71	23.29	5

Table 1 Mixture compositions in wt.%
1. táblázat Keverék összetételek tömegszázalékban

The GFRE additive was obtained by mechanical grinding of composite waste and was sieved to a particle size below 250 µm. Based on loss-on-ignition tests, the GFRE powder was found to contain approximately 58.42 wt.% glass fiber, which is expected to increase the overall SiO_2 content of the ceramic body.

The proportions of alumina and kaolin were adjusted to achieve an Al_2O_3:SiO_2 molar ratio of 3:2 in the fired product, corresponding to the stoichiometric composition of mullite ($3\ Al_2O_3 \cdot 2\ SiO_2$).

Raw materials were mixed and milled for 20 minutes at 200 rpm using a Retsch PM 400 planetary ball mill. The homogenized powders were compacted by uniaxial pressing using a hydraulic press to form test specimens with a diameter of 25 mm.

Heat treatment was carried out in a Nabaltech laboratory electric kiln. Sintering was performed at 1150 °C and 1250 °C for both the reference and GFRE-containing compositions (*Fig. 1*). Additionally, a reference sample (without additive) was sintered at 1400 °C to serve as a benchmark for mullite formation at elevated temperature.

The firing schedule was designed to enable complete burnout of the organic epoxy matrix and to facilitate phase transformation and microstructural development. Following sintering, the samples were analyzed by X-ray diffraction (XRD) to identify crystalline phases and by scanning electron microscopy (SEM) to observe fracture surface morphology and microstructural evolution.

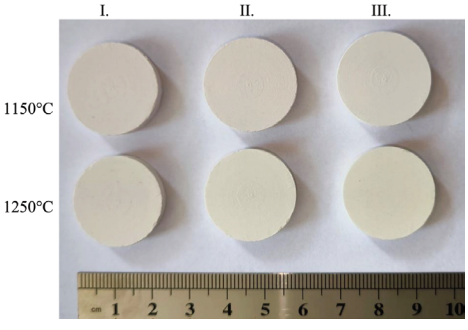

Fig. 1 The sintered test samples
1. ábra A szinterelt próbatestek

3. Results and discussions

Fig. 2 presents the bulk density of the sintered ceramic samples as a function of the heat treatment temperature for both the reference and GFRE-containing compositions. As expected, an increase in sintering temperature led to a corresponding increase in the bulk density of all samples, indicating enhanced sintering activity and the development of a more compact microstructure.

Notably, the addition of GFRE powder consistently reduced the density of the sintered products across all temperatures. This trend appears linear and can be attributed to the partial burnout of the organic epoxy matrix during firing, which increases porosity. The presence of glass fibers may also influence the packing behavior and inhibit full densification. These findings suggest that while GFRE may contribute silica for mullite formation, it simultaneously introduces structural features that limit densification.

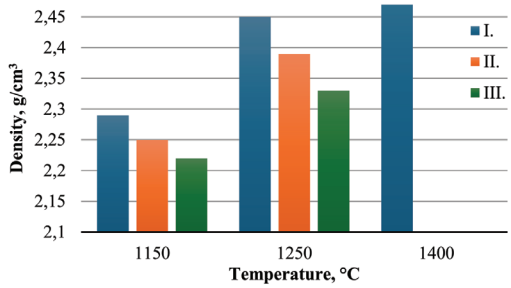

Fig. 2 The density of the sintered ceramic samples
2. ábra A szinterelt próbatestek sűrűsége

The microstructural evolution of the Type I (reference) samples sintered at different temperatures is shown in *Fig. 3*. The SEM images clearly indicate that, as the firing temperature increases, the ceramic particles become more interconnected, reflecting enhanced sintering and grain coalescence.

EDS analysis revealed that a portion of the alumina added to the kaolin remained in its original form within the microstructure. This indicates that not all of the alumina participated in the mullitization reaction during the heat treatment, especially at lower temperatures. Unreacted alumina grains were typically observed embedded within the ceramic matrix, distinguishable by their relatively high aluminum content.

At 1400 °C, the formation of mullite became more apparent, and regions exhibiting needle-like mullite crystals could be observed, which are characteristic of advanced mullitization. These elongated features suggest the onset of secondary mullite growth, commonly associated with higher firing temperatures and partial liquid-phase formation.

Elemental and oxide compositional analysis showed that the overall chemical composition of the samples remained relatively stable across the firing temperature range, with no significant elemental segregation or loss detected.

The SEM images of the GFRE-containing samples reveal the presence of numerous elongated and irregularly shaped pores, especially at higher firing temperatures (*Fig. 4*). These features are likely the result of thermal decomposition and burnout of the organic epoxy matrix within the GFRE additive. The morphology and distribution of these pores suggest that the combustion of the polymer phase created channels or voids aligned with the original fiber orientation.

Despite the increased porosity, the ceramic matrix itself appears more homogeneous and continuous compared to the reference samples. This visual impression may indicate

a higher proportion of amorphous glassy phase, possibly originating from the partial melting of the glass fibers during sintering. Such an increase in glassy phase content could also enhance viscous flow, promoting local densification and phase integration.

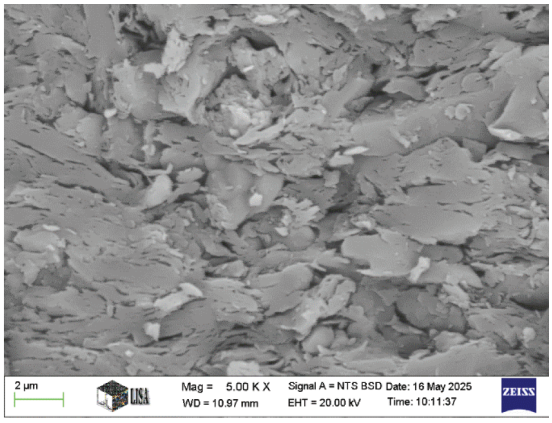

I-1150

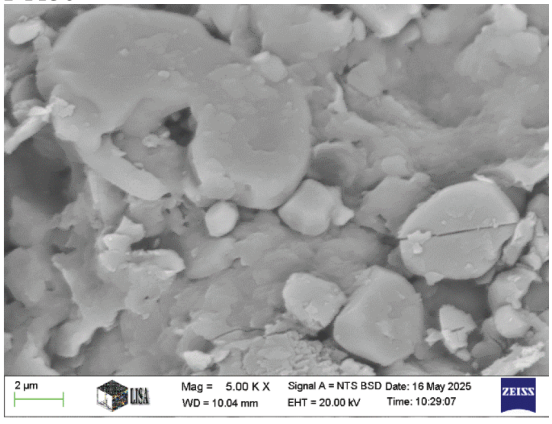

I-1250

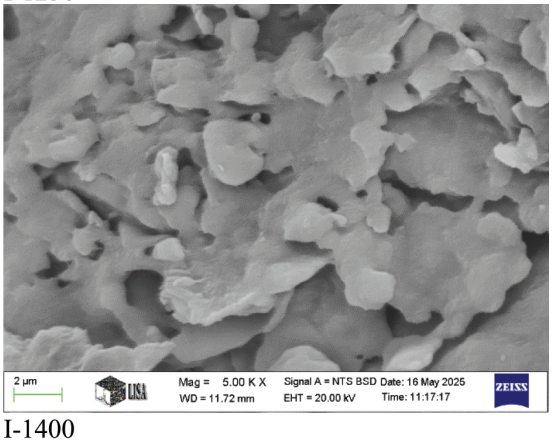

I-1400

Fig. 3 The microstructure of fracture surface of the Type I (reference) samples
3. ábra Az I. típusú (referencia) minták töretfelületének mikroszerkezete

In some of the larger pores – approximately 2 to 2.5 µm in diameter – residual elongated fragments with high SiO_2 content were identified via EDS. These are presumed to be remnants of glass fibers that were only partially decomposed or encapsulated within the ceramic matrix during sintering. Their persistence suggests that some glass fibers may survive firing under certain thermal conditions, potentially contributing to the local SiO_2 content and influencing mullite formation.

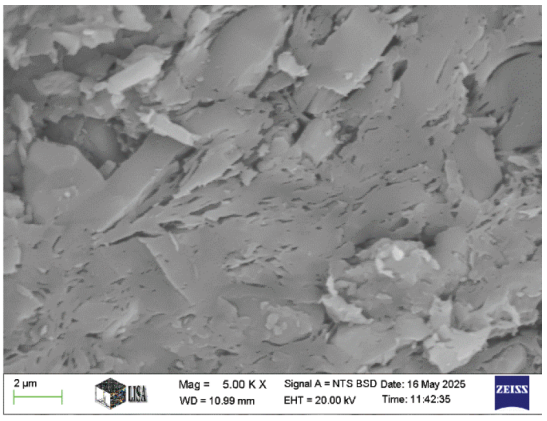

II-1150

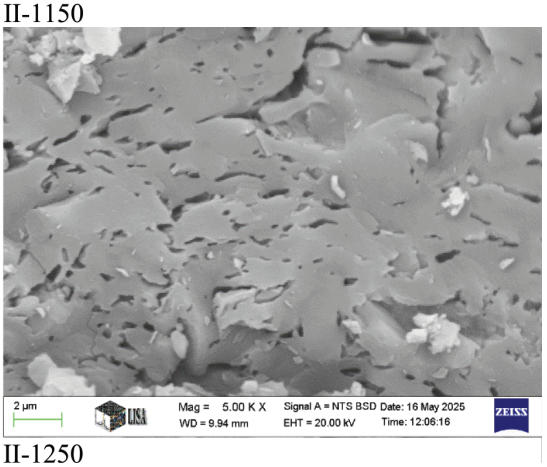

II-1250

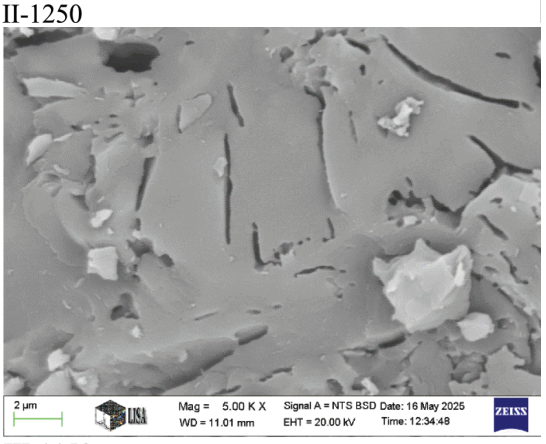

III-1150

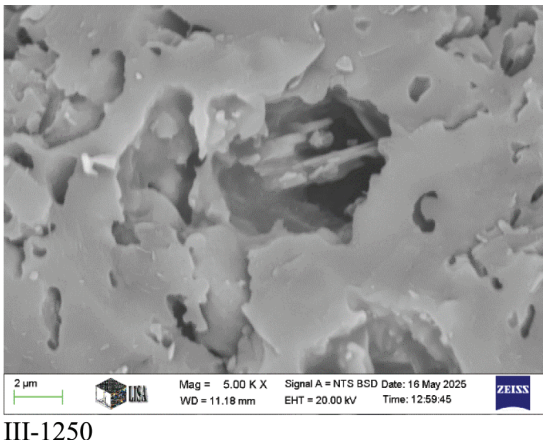

III-1250

Fig. 4 The microstructure of fracture surface of the Type II and III (GFRE-containing) samples
4. ábra Az II. és III. típusú (GFRE tartalmú) minták töretfelületének mikroszerkezete

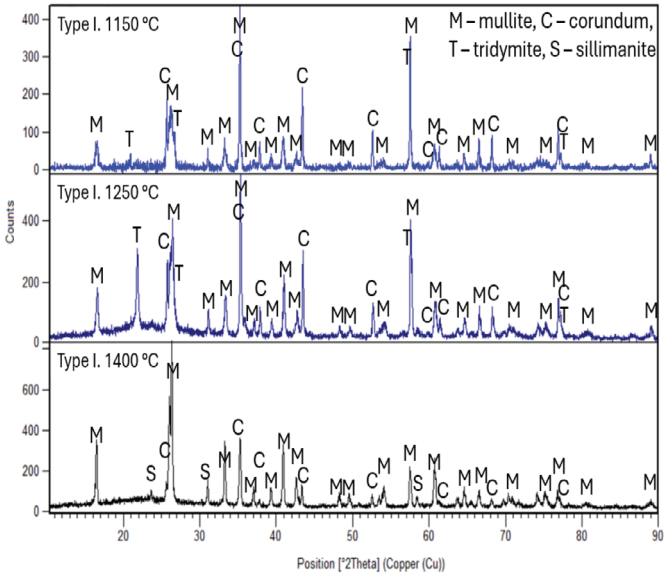

Fig. 5 The XRD pattern of the Type I (reference) samples
5. ábra Az I. típusú (referencia) minták röntgendiffraktogramja

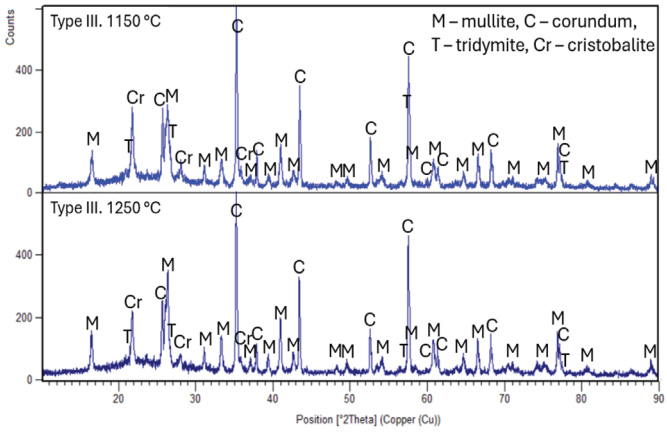

Fig. 6 The XRD pattern of the Type III (GFRE-containing) samples
6. ábra Az II. és III. típusú (GFRE tartalmú) minták röntgendiffraktogramja

Sintering temperature		1150 °C			1250 °C			1400 °C
Type of sample / Mixture sign		I.	II.	III.	I.	II.	III.	I.
Crystalline content, wt.%		41,0	41,8	40,6	58,1	61,3	64,1	74,9
Amorphous content, wt.%		59,0	58,2	59,4	41,9	38,7	35,9	25,1
Crystalline phases, wt.%	Mullite	17,2	24,0	25,0	37,8	36,2	42,3	52,4
	Corundum	14,8	10,6	11,0	16,3	12,3	16,0	11,2
	Tridymite	9,0	3,7	3,8	4,1	7,4	1,3	0,0
	Cristobalite	0,0	2,4	2,5	0,0	6,1	4,5	0,0
	Sillimanite	0,0	0,0	0,0	0,0	0,0	0,0	11,2

Table 2 Phase compositions of the sintered samples
2. táblázat A szinterelt minták fázisösszetétele

The results of the XRD measurements are summarized in *Table 2*, while representative diffractograms are presented in *Fig. 5* and *6*. The effect of sintering temperature on phase composition is clearly observable in all samples.

At 1150 °C, mullite formation had already begun, with a crystalline phase content around 41% in all mixtures. Increasing the sintering temperature to 1250 °C led to a significant rise – by at least 29% – in the total crystalline content across all three compositions, indicating enhanced crystallization and sintering activity.

In general, the GFRE-containing samples (Type II and III) exhibited a higher proportion of crystalline phases compared to the additive-free reference (Type I) at each temperature. This may be due to the glass fiber content of the GFRE additive, which includes amorphous silica that can crystallize upon slow cooling. As a result, cristobalite and tridymite phases appeared specifically in the GFRE-containing ceramics, likely formed from the devitrification of the residual glass.

Mullite was the dominant crystalline phase in all samples, and its quantity increased steadily with temperature. The presence of unreacted corundum (α- Al_2O_3) in each composition suggests that not all of the alumina participated in the mullitization reaction. Part of the alumina likely reacted with the tridymite generated during kaolin dehydration, and with glass-derived silica in the GFRE-containing systems, contributing to mullite formation.

At 1250 °C, mullite content reached 37.8% in the reference and up to 42.3% in GFRE-added mixtures, indicating that this temperature may be optimal for mullite synthesis under the given conditions. At 1400 °C, mullite formation peaked (52.4%), and sillimanite appeared in the reference sample, likely due to phase transitions at elevated temperature.

Overall, these results confirm that GFRE not only supports mullite crystallization but may also enhance overall crystallinity by contributing reactive SiO_2, while also introducing secondary silica phases due to partial devitrification of glass fibers.

4. Conclusions

This study demonstrated the feasibility of using mechanically ground glass fiber-reinforced epoxy (GFRE) waste as an additive in kaolin–alumina-based mullite ceramic systems. The following key conclusions can be drawn:

- The incorporation of GFRE powder led to a consistent decrease in the bulk density of the sintered ceramics due to the formation of elongated pores, originating from the burnout of the organic matrix.
- SEM analysis confirmed the development of a more continuous and interconnected ceramic network in the GFRE-containing samples, likely promoted by the presence of amorphous glassy phases derived from the melted glass fibers.
- XRD results showed that mullite formation occurred in all compositions and increased with sintering temperature. At 1150–1250 °C, GFRE-containing samples exhibited slightly higher mullite content than the additive-free reference, indicating that the recycled additive can serve as a reactive silica source.

- The presence of cristobalite and tridymite in the GFRE samples, as well as unreacted corundum across all compositions, suggests that phase evolution is influenced by both the additive composition and firing conditions.
- An optimal sintering temperature of 1250 °C was identified for promoting mullite formation while balancing porosity and crystallinity.

Overall, the results confirm that recycled GFRE waste can be effectively reused in the production of mullite ceramics, contributing both reactive components and structural modifications. This approach supports sustainable ceramic manufacturing and offers a practical valorization route for difficult-to-recycle composite materials.

Acknowledgement

„Supported by the University Research Scholarship Program of the Ministry for Culture and Innovation from the source of the National Research, Development and Innovation Fund."

References

[1] Romero M, Padilla I, Contreras M, López-Delgado A. Mullite-Based Ceramics from Mining Waste: A Review. Minerals. 2021, 11(3) p.332. https://doi.org/10.3390/min11030332

[2] Behera P.S., Bhattacharyya S. Sintering and microstructural study of mullite prepared from kaolinite and reactive alumina: Effect of MgO and TiO_2, International Journal of Applied Ceramic Technology, 2020, 17(2), pp. 560–572, https://doi.org/10.1111/ijac.13637

[3] Ma J. et al., Low-temperature synthesis of highly porous whisker-structured mullite ceramic from kaolin, Ceramics International, 2018, 44(11), pp. 13320–13327, https://doi.org/10.1016/j.ceramint.2018.04.163

[4] Ptáček P., The kinetics and mechanism of kaolin powder sintering I, Powder Technology, 2012, 232, pp. 24–32, https://doi.org/10.1016/j.powtec.2012.07.060

[5] Chen Y-F., Wang M-C., Hon M-H., Phase transformation and growth of mullite in kaolin ceramics, Journal of the European Ceramic Society, 2004, 24(8), pp. 2389–2397, https://doi.org/10.1016/S0955-2219(03)00631-9

[6] Choo T.F. et al., A review on synthesis of mullite ceramics from industrial wastes, Recycling, 2019 4(3), pp. 39–63, https://doi.org/10.3390/recycling4030039

[7] Foo C.T. et al., Mineralogy and thermal expansion study of mullite-based ceramics synthesized from coal fly ash and aluminum dross industrial wastes, Ceramics International, 2019, 45(5), pp. 7488–7494, https://doi.org/10.1016/j.ceramint.2019.01.041

[8] Alves H.P.A. et al., Preparation of mullite based ceramics from clay–kaolin waste mixtures, Ceramics International, 2016, 42(16), pp. 19086–19090, https://doi.org/10.1016/j.ceramint.2016.09.068

[9] Silva V.J. et al., Porous mullite blocks with compositions containing kaolin and alumina waste, Ceramics International, 2016, 42(12), pp. 15471–15478, https://doi.org/10.1016/j.ceramint.2016.06.199

[10] Kocserha I., Hamza A., Géber R., The effects of red mud on clay compounds, IOP Conference Series: Materials Science and Engineering, 2018, 426, 012026, https://doi.org/10.1088/1757-899X/426/1/012026

[11] Ji H. et al., Effect of La_2O_3 additives on the strength and microstructure of mullite ceramics obtained from coal gangue and γ-Al2O3, Ceramics International, 2013, 39(6), pp. 6841–6846, https://doi.org/10.1016/j.ceramint.2013.02.016

[12] Zhang J. et al., Mechanism of mechanical–chemical synergistic activation for preparation of mullite ceramics from high-alumina coal fly ash, Ceramics International, 2018, 44(3), pp. 3884–3892, https://doi.org/10.1016/j.ceramint.2017.11.178

[13] Sahraoui T., Belhouchet H., Heraiz M., Brihi N. Guermat A., The effects of mechanical activation on the sintering of mullite produced from kaolin and aluminum powder, Ceramics International, 2016, 42(10), pp. 12185–12193, https://doi.org/10.1016/j.ceramint.2016.04.157

[14] Rashad M., Balasubramanian M., Characteristics of porous mullite developed from clay and $AlF_3{\cdot}3H_2O$, Journal of the European Ceramic Society, 2018, 38(11), pp. 3673–3680, https://doi.org/10.1016/j.jeurceramsoc.2018.03.002

[15] Ibrahim J.F.M., Gömze A.L., Koncz-Horvath D., Filep Á., Kocserha I., Preparation, characterization, and physicomechanical properties of glass-ceramic foams based on alkali-activation and sintering of zeolite-poor rock and eggshell, Ceramics International, 2022, 48(18), pp. 25905-25917 https://doi.org/10.1016/j.ceramint.2022.05.267

[16] Guangfa Gao, Yongchi Li, Mechanical Properties of Woven Glass-Fiber Reinforced Polymer Composites, Emerging Materials Research 5(2) http://dx.doi.org/10.1680/jemmr.16.00018

[17] Shubham Utekar, Suriya V K, Neha More, Adarsh Rao, Comprehensive study of recycling of thermosetting polymer composites – Driving force, challenges and methods, Composites Part B: Engineering, 2021, 207, 108596, https://doi.org/10.1016/j.compositesb.2020.108596

[18] Xu M-X. et al., Insights into the pyrolysis mechanisms of epoxy resin polymers based on the combination of experiments and ReaxFF-MD simulation, Chemical Engineering Journal, 2023, 473, 145404, https://doi.org/10.1016/j.cej.2023.145404

[19] López F.A. et al., Recycling of Glass Fibers from Fiberglass Polyester Waste Composite for the Manufacture of Glass-Ceramic Materials, Journal of Environmental Protection, 2012, 03(08) pp.740-747. http://dx.doi.org/10.4236/jep.2012.38088

[20] Ondro J. et al., Kinetic analysis of sinter-crystallization of mullite and cristobalite from kaolinite, Thermochimica Acta, 2019, 678, pp. 30–37, https://doi.org/10.1016/j.tca.2019.178312

[21] Badanoiu A., Influence of Synthesis Route on Composition and Main Properties of Mullite Ceramics Based on Waste, MDPI Materials, 2025, 18(5), pp. 1098–1112, https://doi.org/10.3390/ma18051098

[22] Mohamed L.J. et al., Effect of sintering temperatures on the physical, structural properties and microstructure of mullite-based ceramics, AIMS Materials Science, 2024, 11(2), pp. 243–255, https://doi.org/10.3934/matersci.2024014

[23] Behera P.S., Bhattacharyya S., Effect of different alumina sources on phase formation and densification of single-phase mullite ceramic – Reference clay alumina system, Materials Today Communications, 2021, 26, 101818, https://doi.org/10.1016/j.mtcomm.2020.101818

[24] Aziz A.A., Fabrication and characterization of mullite ceramic hollow fiber membrane from natural occurring ball clay, Applied Clay Science, 2019, 177, pp.51–59, https://doi.org/10.1016/j.clay.2019.05.003

[25] Gonçalves R. M., Martinho A., Oliveira J. P., Recycling of Reinforced Glass Fibers Waste: Current Status, MDPI Materials (Basel), 2022, 15(4), 1596, https://doi.org/10.3390/ma15041596

[26] Li Junfeng, Lin Hong, Li Jianbao, Wu Jiang, Effects of different potassium salts on the formation of mullite as the only crystal phase in kaolinite, Journal of the European Ceramic Society, 2009, 29(14), pp.2929–2938, https://doi.org/10.1016/j.jeurceramsoc.2009.04.032

[27] Chen Y., Effect of quartz and muscovite on mullite formation, Applied Clay Science, 2013, 80–81, pp.176–184, https://doi.org/10.1016/j.clay.2013.04.008

Ref.:
Kurovics, Emese – **Mnichl**, Habtamu – **Tokár**, Monika: *Use of recycled glass fiber–epoxy resin as additive for mullite ceramics*
Építőanyag – Journal of Silicate Based and Composite Materials, Vol. 77, No. 2 (2025), 55–59 p.
https://doi.org/10.14382/epitoanyag-jsbcm.2025.8

GUIDELINE FOR AUTHORS

The manuscript must contain the followings: title; author's name, workplace, e-mail address; abstract, keywords; main text; acknowledgement (optional)**; references; figures, photos with notes; tables with notes; short biography** (information on the scientific works of the authors).

The full manuscript should not be more than 6 pages including figures, photos and tables. Settings of the word document are: 3 cm margin up and down, 2,5 cm margin left and right. Paper size: A4. Letter size 10 pt, type: Times New Roman. Lines: simple, justified.

TITLE, AUTHOR

The title of the article should be short and objective.

Under the title the name of the author(s), workplace, e-mail address.

If the text originally was a presentation or poster at a conference, it should be marked.

ABSTRACT, KEYWORDS

The abstract is a short summary of the manuscript, about a half page size. The author should give keywords to the text, which are the most important elements of the article.

MAIN TEXT

Contains: materials and experimental procedure (or something similar), results and discussion (or something similar), conclusions.

REFERENCES

References are marked with numbers, e.g. [6], and a bibliography is made by the reference's order. References should be provided together with the DOI if available.

Examples:

Journals:

[6] Mohamed, K. R. – El-Rashidy, Z. M. – Salama, A. A.: In vitro properties of nano-hydroxyapatite/chitosan biocomposites. *Ceramics International.* 37(8), December 2011, pp. 3265–3271, http://doi.org/10.1016/j.ceramint.2011.05.121

Books:

[6] Mehta, P. K. – Monteiro, P. J. M.: Concrete. Microstructure, properties, and materials. *McGraw-Hill*, 2006, 659 p.

FIGURES, TABLES

All drawings, diagrams and photos are figures. The **text should contain references to all figures and tables**. This shows the place of the figure in the text. Please send all the figures in attached files, and not as a part of the text. **All figures and tables should have a title**.

Authors are asked to submit color figures by submission. Black and white figures are suggested to be avoided, however, acceptable.

The figures should be: tiff, jpg or eps files, 300 dpi at least, photos are 600 dpi at least.

BIOGRAPHY

Max. 500 character size professional biography of the author(s).

CHECKING

The editing board checks the articles and informs the authors about suggested modifications. Since the author is responsible for the content of the article, the author is not liable to accept them.

CONTACT

Please send the manuscript in electronic format to the following e-mail address: femgomze@uni-miskolc.hu and epitoanyag@szte.org.hu or by post: Scientific Society of the Silicate Industry, Budapest, Bécsi út 122–124., H-1034, HUNGARY

We kindly ask the authors to give their e-mail address and phone number on behalf of the quick conciliation.

Építőanyag – *Journal of Silicate Based and Composite Materials*, Quarterly peer-reviewed periodical of the Hungarian Scientific Society of the Silicate Industry, SZTE.
http://epitoanyag.org.hu